Dynamic Organic Room-Temperature Phosphorescent Systems

Qian Zhou,[1] Chaolong Yang[1,2]*, Yanli Zhao[2]*

[1]School of Materials Science and Engineering, Chongqing University of Technology, Chongqing, 400054. Email: yclzjun@163.com

[2]School of Chemistry, Chemical Engineering and Biotechnology, Nanyang Technological University, 21 Nanyang Link, Singapore 637371. Email: zhaoyanli@ntu.edu.sg

SUMMARY: Organic room-temperature phosphorescent (RTP) systems can be divided into dynamic and static organic phosphorescent materials based on their response mode to external stimuli. Dynamic organic phosphorescent materials are more useful compared to conventional static RTP materials owing to their reversible sensitivity, quick response, and ease of controlling their properties. With the rapid development of organic RTP systems, dynamic organic RTP materials are expected to meet the practical requirements. Herein, we review the recent research progress on dynamic organic RTP systems by (1) direct visual monitoring of phosphorescent intensity and color changes under external stimuli and (2) providing insights into the relationship between molecular response modes and different response behavior. In particular, strategies for enhancing RTP performance and tuning phosphorescence colors are highlighted. The prospects and future challenges in this promising field are also discussed to promote the further development of advanced dynamic organic RTP systems.

Keywords: Afterglow; Dynamic organic room-temperature phosphorescence; Intermolecular interactions; Phosphorescence performance; Stimuli-responsive properties

INTRODUCTION

Phosphorescence emission, a unique and long-lived photoluminescence phenomenon, has always attracted interest of both the general public and the scientific community. Unlike the record of inorganic phosphorescence dating back to centuries, the documented reports on

organic phosphorescence could only be traced back to the 1930s when Clapp observed that the bright green to blue afterglow from solid crystalline tetraphenylmethane and tetraphenylsilane derivatives at room temperature lasted for 23 s and considered that trace impurities in the solid could be responsible for the afterglow emission.[1] Since then, organic phosphorescence has attracted extensive interest and in-depth exploration because of its long-lived triplet excitons and large Stokes shifts. Organic phosphorescent materials are widely used in bioimaging, organic light-emitting diodes, dynamic light therapy, data encryption and anti-counterfeiting, chemical and biological sensing, and other such fields.[2-6] In recent years, the demand for pure organic room-temperature phosphorescent (RTP) materials has increased, which has led to the development of many effective strategies to successfully achieve remarkable emissions from pure organic RTP materials. These strategies usually involve host–guest interactions,[7] crystallization,[8] and heavy-atom effects,[9] as well as embedding phosphors into a polymer matrix or synthesizing phosphors containing polymer chains.[10,11]

Rapid development of organic RTP materials has led to the emergence of smart materials with dynamic phosphorescence performances. When external stimuli are applied to RTP materials, static RTP materials exhibit only macroscopic changes, while molecular microscopic changes become essentially nonexistent. Additionally, the corresponding photophysical properties do not change. In contrast, dynamic RTP materials exhibit both macroscopic and microscopic structural changes, which in turn change the optical and physical properties of these materials. Therefore, static RTP materials exhibit phosphorescence emission of a certain color under instantaneous ultraviolet (UV) light excitation. When a series of external stimuli, such as UV light irradiation for a long duration, heating or cooling, grinding, or dissolution, are applied to static RTP materials, their temperature or physical state changes accordingly. However, their photophysical properties do not change even under UV light excitation. Unlike the nontunable photophysical properties of static RTP materials, the physical properties of dynamic organic RTP materials, such as the phosphorescence color, intensity, lifetime, and quantum yield, can be tuned under external stimuli, changing both the external and internal states of these materials along with their stimuli-responsive characteristics. Owing to their superior reversible sensitivity, quick

response, and easy control, dynamic RTP materials have advantages over conventional static RTP materials. However, it is very difficult to develop dynamic RTP materials, because it is almost impossible to simultaneously control triplet excitons and stimulus-response sites.[12] Thankfully, with the continuous efforts of scientists, some exciting research progress has been made in this field.[13-16] Huang et al. demonstrated a simple organic molecular crystal display with both mechanoluminescence and photo-induced RTP.[14] Yang et al. reported large-area and flexible polymer-based transparent films with temperature-dependence afterglow through dual emission of thermally activated delayed fluorescence and ultralong organic phosphorescence (UOP).[15] Li et al. realized pure organic amorphous polymeric phosphorescence materials showing full-color tunability under different excitation wavelengths.[16] However, dynamic RTP is still in the initial stage, and many issues such as how to obtain an ideal dynamic afterglow performance by effectively regulating molecular motion modes need to be resolved. In addition, it remains a formidable challenge to explore a simple and efficient approach for obtaining dynamic RTP materials with excellent photophysical features.

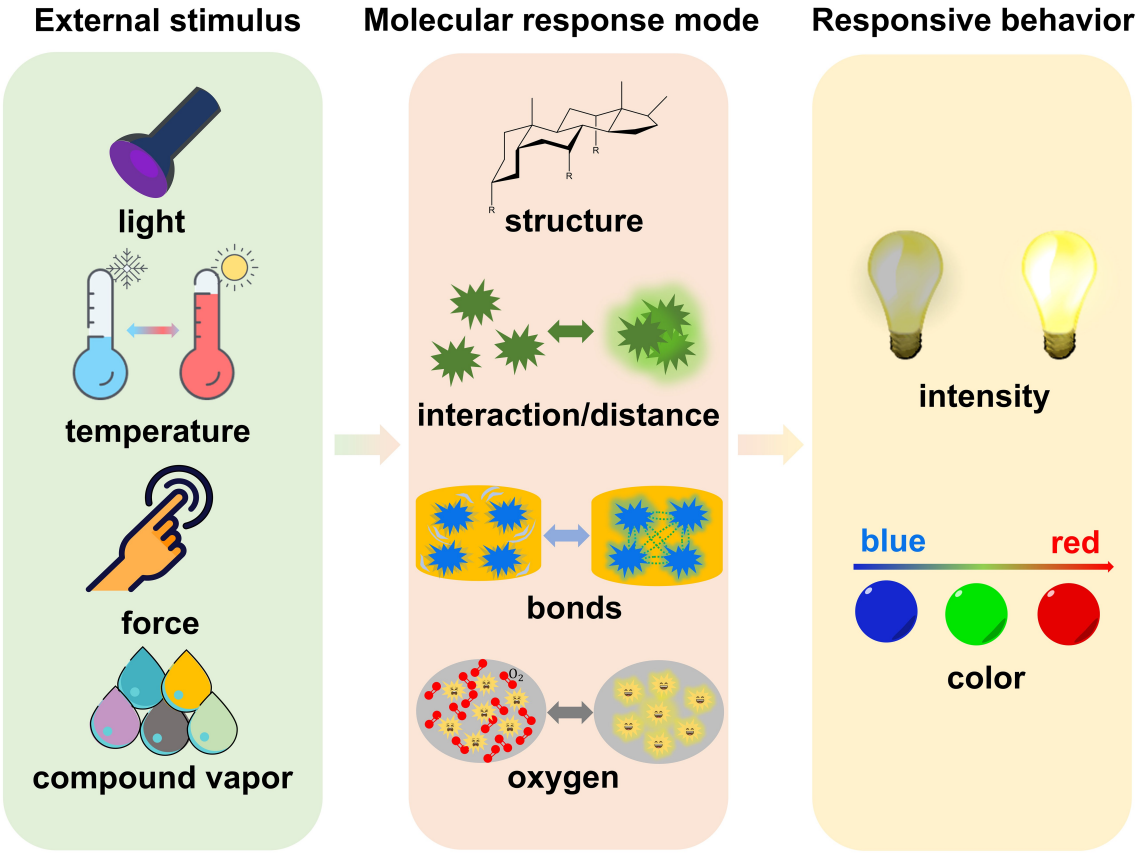

Figure 1. Schematic illustration of dynamic organic RTP materials.

Molecules exhibit different answered modes under an external stimulus with distinct

phosphorescence-responsive behavior.

This review conducts a direct visual monitorization of phosphorescence intensity and color changes under external stimuli[17] and discusses dynamic organic RTP materials by focusing on their emission intensity and phosphorescence color caused by microscopic changes at the molecular level under external stimuli. Microscopic changes within materials usually manifest as structural diversification, interaction or changes in the distance among molecules, appearance and disappearance of some bonds between molecules, and a decrease in the oxygen content around molecules. As shown in **Figure 1**, when external stimuli are applied to dynamic RTP materials, microscopic changes occur at the molecular level within the material, leading to molecular responses in the form of changes in the photophysical properties of the material, which are reflected in both the phosphorescence intensity and color. We also highlight the major problems and possible solutions for further developing dynamic RTP materials.

PHOSPHORESCENCE EMISSION FROM DUSK TO BRIGHT

Intense intermolecular interactions enhancing RTP

Small organic molecules usually tend to have stable triplet excitons and suppress nonradiative transitions through a rigid crystal environment.[18,19] However, tight molecular packing modes would partially hinder molecular motion under external stimuli, resulting in molecules with nontunable photophysical properties. Nevertheless, some small-molecule systems with dynamic RTP have been developed by utilizing changeable intermolecular interactions caused by molecular motion.

Boron-containing materials have been extensively investigated because of their intense fluorescence and superior RTP.[20,21] However, their investigation requires strict conditions, such as determining the appropriate molecular weight or optimum polymer ratio, even in a rigid environment, to realize the best RTP. This limits the scope of their application. Chai et al. synthesized a series of aryl boronic acids with a lifetime of up to 2.24 s in the crystal state.[22] These boron-containing materials exhibit long-lived RTP without needing any complex adjustments. For example, 4-methoxyphenylboronic acid (PBA-MeO) shows that hydrogen

bonds strengthen the intermolecular interactions, resulting in the formation of denser molecular packing[23] and crystals. Rigid conformation and stable triplet excitons of PBA-MeO, which is controlled by effective π–π stacking, decrease the nonradiative decay, resulting in ultralong RTP with a lifetime of 2.24 s. However, this material is highly unstable. As the temperature increases, phenyl boric acid converts to triphenyl boroxine (tPBA) through dehydration (**Figure 2A**).[24] The higher plane angle (increased from 70.6° to 79.1°) and longer distance (increased from 2.0 to 3.39 Å) between the adjacent layers result in rapid nonradiative deactivation of triplet excitons, resulting in RTP with weak intensity and short lifetime. Although the molecular structure of PBA–MeO changed after dehydration, this change was reversible under fumigation with water vapor, which helped in the recovery of the initial RTP-emission intensity. In contrast, when the alkoxy group was changed to a halo group (PBA-*x*, *x*: F, Cl, Br, or I), the phosphorescence properties of tPBA-*x* improved after heating. For PBA-Br, the lifetime increased from 73 to 170 ms and bright yellow phosphorescence was observed after dehydration, owing to intense π–π stacking interactions that increase the phosphorescence intensity and lifetime of tPBA-Br. Because of these properties, the authors applied these materials to secure encryption. As shown in **Figure 2B**, before heating and when the UV irradiation was switched off, only the word "CHEM" exhibited green phosphorescence, while after heating at 80 °C for 2 h, they all dehydrated, switching on "IS" and "TRY" and switching off "CHEM." Reversible structural changes and dynamic RTP properties of these materials have broadened their application prospects.

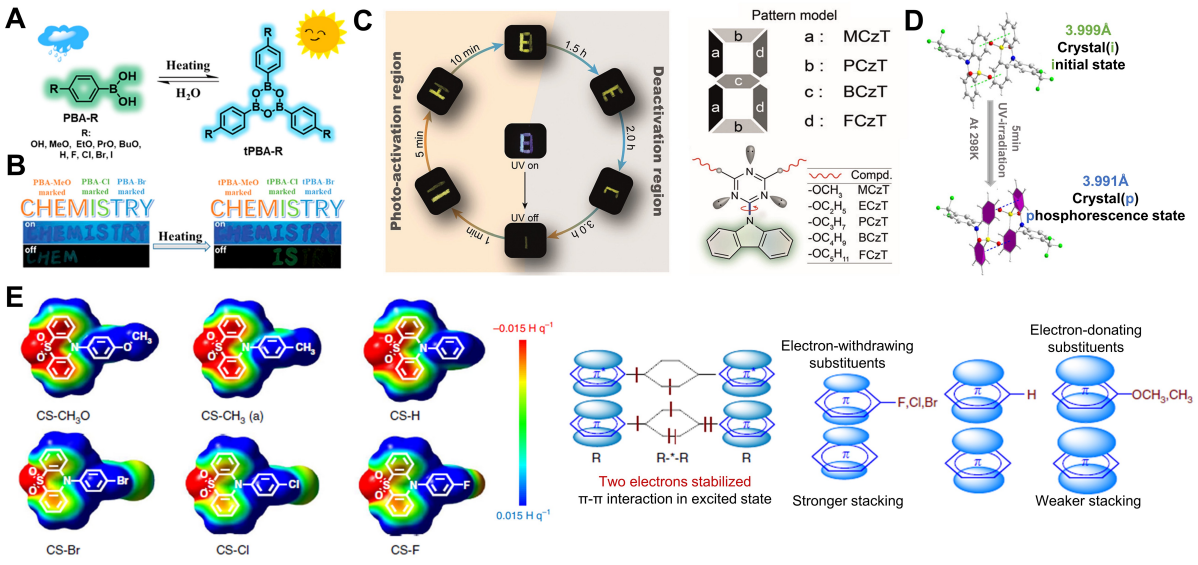

Figure 2. **Small disparity in molecular structures results in dramatically different dynamic response behaviors.**

(A) Molecular structures of PBA-R and tPBA-R under external stimulus-induced interconversion. (B) Encryption application for security document. Reprinted with permission from Chai et al.[22] Copyright 2017 Royal Society of Chemistry. (C) A series of molecular rotors with advanced anti-counterfeiting applications. Reprinted with permission from Gu et al.[26] Copyright 2017 Wiley-VCH Verlag GmbH & Co. KGaA, Weinheim. (D) Changeable crystal structures of CS-CF_3 under UV irradiation. (E) π–π interactions manipulate RTP behavior by regulating the electron redistribution. Reprinted with permission from Yang et al.[27] Copyright 2020 Springer Nature.

To the best of our knowledge, molecular structural designs in previous studies often introduced a series of similar functional groups or units with exponentially increasing carbon chains to obtain compounds with related properties. Because partial molecular motion in crystal state and the molecular stacking of alkyl chains can be manipulated rationally,[25] Gu et al. designed and prepared a series of molecules containing a carbazole unit, a triazine core, and alkoxyl chains of different lengths.[26] Under UV excitation, all five compounds (MCzT, ECzT, PCzT, BCzT, and FCzT) exhibited blue emission. Only MCzT and ECzT emitted yellow phosphorescence that lasted for several seconds after irradiation. PCzT, BCzT, and FCzT exhibited bright ultralong organic phosphorescence upon irradiation for several minutes. They conducted a series of experiments to investigate these unique characteristics. Stronger intermolecular interaction is key for dynamic RTP (from "off" to "on"). Further research on the molecular structure has revealed that the molecular overlap between neighboring molecules gradually decreases with an increase in the length of the alkoxyl chain. Lower molecular overlap results in weak intermolecular interactions; therefore, PCzT, BCzT, and FCzT do not show RTP before photoactivation. However, weak intermolecular interaction endows molecular motion. Thus, after photoactivation, the distance of intermolecular interactions between the neighboring molecules on the same plane decreased; for example, the distance between carbazole and triazine groups decreased from 2.661 and 2.702 Å to 2.635 and 2.677 Å, resulting in intense intermolecular interactions that form stable triplet excitons.

The longer the alkoxy chains, the shorter the photoactivation response time; for example, for FCzT, this time decreased from 7 to 1 min. Additionally, there was a slight change in the molecular configuration owing to the strict suppression of intermolecular interactions, both before and after photoactivation. Consequently, the nearly unchanged molecular configuration and tunable intermolecular interactions under photoactivation play critical roles in dynamic RTP molecules. Because of the molecular motion-induced dynamic RTP, the RTP recovered to the initial stage when the molecule was heated at 338 K for 5 min or maintained at room temperature. Given the dynamic RTP property with reversible sensitivity and varied photoactivation time for MCzT, BCzT, and PCzT, they fabricated an anti-counterfeiting pattern "8" to exhibit different numbers under varied photoactivation (**Figure 2C**).

Another very interesting example of the dynamic RTP system was explored based on the changed molecular packing and strong intermolecular π−π interaction. Yang et al. designed six 10-phenyl-10H-phenothiazine-5,5-dioxide-based derivatives with different RTP effects.[27] Among these derivatives, three had an electron-withdrawing substituent group on the 10-phenyl ring (CS−F, CS−Cl, and CS−Br), two had an electron-donating substituent on the 10-phenyl ring (CS−CH_3O and CS−CH_3), and one was without any substituent (CS−H). To explore how different substituent groups influence the RTP behavior of these compounds, their corresponding spectra were measured in both the crystal state and dichloromethane solution. In the dichloromethane solution, the six compounds exhibited similar behaviors. However, there were obvious differences in their RTP spectra and lifetimes; for example, the lifetimes were 268 ms (CS−Br), 256 ms (CS−Cl), 410 ms (CS−F), 188 ms (CS−H), 96 ms (CS−CH_3), and 88 ms (CS−CH_3O). Based on the difference between the crystal and dichloromethane states, the different RTP behaviors of the six compounds may be ascribed to the molecular packing mode. An analysis of the crystal structure demonstrated that the three compounds, CS−F, CS−Cl, and CS−Br, with the centroid−centroid distance between them ranging from 3.677 to 3.732 and 3.773 Å, bring about strong π−π stacking. The distances were tuned from 3.994 Å to 4.296, 4.116, and 4.251 Å for CS−H, CS−CH_3, and CS−CH_3O, respectively. The above data reveal the corresponding association of the substituent groups with the stacking mode. The π–π interaction of the electron−acceptor substituent was stronger than that of the other two, while the electron−donor substituent showed the weakest π−π

interactions. Therefore, strong π–π interactions between molecules are key to stabilizing triplet excitons with an ultralong RTP. Research on the influence of electronic effects on π–π interactions further demonstrated the positive effect of electron-withdrawing substituents on strong π–π interactions. The electron-withdrawing substituents could decrease the π-electron density of the substituted π-system, alleviate the π–π repulsion between the adjacent rings, and finally result in intense π–π stacking. In contrast, electron donation weakens π–π interactions. Furthermore, the electron density on the phenyl ring gradually increased owing to the change from electron-withdrawing and no-substituent groups to electron-donating substituents. The real-space electron density can relieve the π–π repulsion, which shortens the π–π distance and enhances π–π interactions. Taking advantage of the excellent RTP induced by electron-withdrawing groups, they introduced a trifluoromethyl group with a stronger withdrawing ability (**Figure 2D, E**). Surprisingly, the CS–CF_3 crystal exhibited reversible irradiation-dependent RTP, owing to a reversible change in molecular packing. The distance between the two phenyl rings in $CSCF_3$ changed from 3.9995 to 3.991 Å after irradiation with 365-nm UV light for 5 min. Although the change in the π–π distance is small, it plays a critical role in enhancing the π–π interactions. Consequently, good RTP owing to the introduction of an electron-withdrawing group may allow molecular design of ultralong RTP materials.

Volatile organic compounds (VOCs) are widely present in daily life. However, some VOCs are toxic and can threaten health and life. To date, only a few dynamic RTP materials have been developed for VOC detection based on their fast responsive characteristics with the RTP turn “on” or “off” and color changes. Wu et al. reported an organic compound, 2,4-di(10H-phenothiazin-10-yl)-1,3,5-triazine (TDP), which can tune its RTP “on” to “off” in the presence of toxic chloroform vapor.[28] To better study the dynamic changes of TDP, authors cultivated two different single crystals, TDP-EA (cultivated through ethyl acetate) and TDP-CF (chloroform), to simulate the molecular structure before and after chloroform fumigation, respectively. TDP-EA can emit bright green phosphorescence up to 56 ms, owing to the rigid environment resulting from multiple strong intermolecular interactions such as C–H···S (2.945 and 2.961 Å), C–H···π (2.745 and 2.814 and 3.192 Å), and C–H···N (2.628 Å). In contrast, one TDP molecule containing two chloroform molecules in the TDP-CF crystal

formed looser molecular packing with weak layer-by-layer interactions and reduced intermolecular interactions, resulting in a faster nonradiative rate. Therefore, the phosphorescence of TDP-CF was quenched with chloroform. To gain a deeper understanding of these changes, factors influencing the phosphorescence lifetime (τ_p) were studied. According to the equation $\tau_p = 1/(K_r + K_{nr})$, the nonradiative ($K_{nr}$) and radiative ($K_r$) decay rates with τ_p show a negative correlation. After fuming with chloroform vapor, the reorganization energy increased from 0.51 to 0.53 eV and spin-orbit coupling from T_1 to S_0 prolonged from 7.00 to 10.96 cm^{-1} owing to the looser molecular arrangement. These two factors enhance K_{nr}. Simultaneously, enhanced oscillator strength (f_T, from 8.36×10^{-8} to 3.8×10^{-8}) increases the K_r of triplet excitons. The enlarged K_r and K_{nr} lower the phosphorescence lifetime and cause RTP to change from "on" to "off." Under heating or vacuum treatment at room temperature, RTP returns to the initial stage when chloroform is removed. Using a dynamic phosphorescence switch, a visual probe was developed to detect chloroform concentrations with a low detection limit of approximately <5 ppm. Inspired by this aspect, in 2021, Gao et al. also realized dynamic RTP by dichloromethane fumigation.[29] After being fumed, the PTZ-3Cl-ax conformer could turn to PTZ-3Cl-eq with the phosphorescence emission switching from "off" to "on." These two interconverted conformations (ax and eq) are the main reasons for the stimuli-responsive behavior of the compound (**Figure 3A, B**).

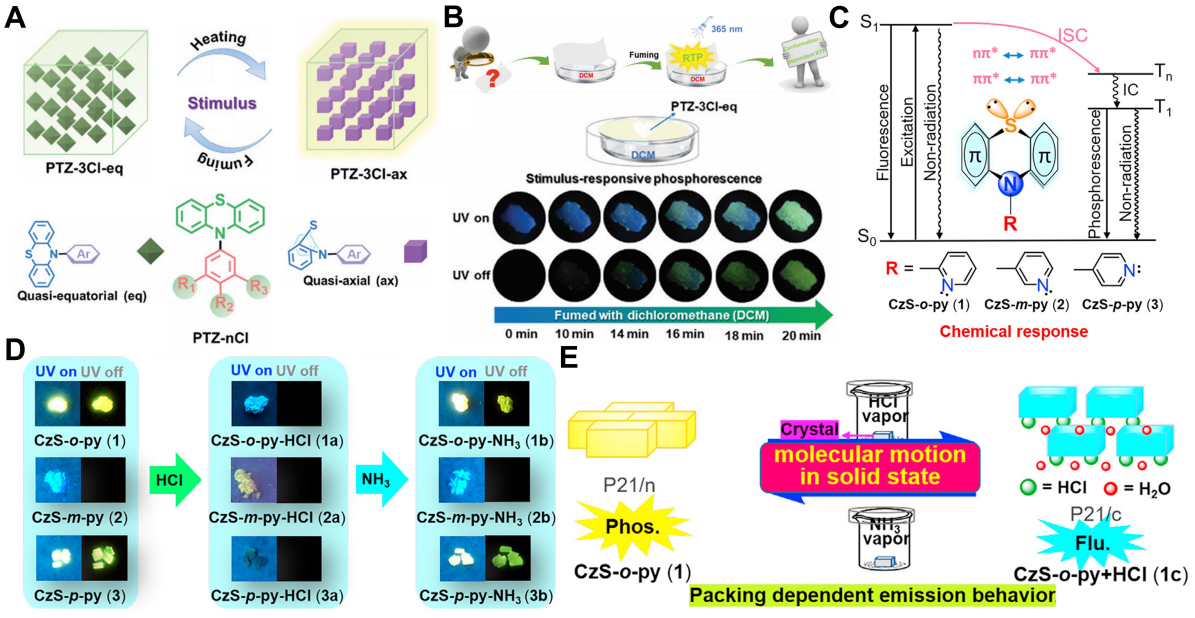

Figure 3. VOCs for inducing reversible RTP behavior.

(A) Reversible conformational changes of PTZ-3Cl stimulated by dichloromethane fumigation and heating. (B) Turning on the RTP effect under dichloromethane fumigation. Photographs show the fluorescence and phosphorescence states of PTZ-3Cl. Reprinted with permission from Gao et al.[29] Copyright 2021 Royal Society of Chemistry. (C) Representation of structural design strategy. (D) Fluorescence and phosphorescence images of CzS-*o*-py crystals after fumigation with hydrochloric acid and ammonia. (E) Schematic representation of molecular motion under the stimuli of hydrochloric acid and ammonia. Reprinted with permission from Tian et al.[30] Copyright 2020 The Author(s).

Besides VOCs, the stimulation of acid/base to alter the excited state of phosphors is also an efficient method to adjust the molecular packing and the corresponding RTP performance. In 2020, Tian et al. synthesized three stimulus-responsive molecules under hydrochloric acid-vapor fuming[30] by integrating phenothiazine and isomeric pyridine groups to produce the organic molecules CzS-*o*-py (1), CzS-*m*-py (2), and CzS-*p*-py (3). Phenothiazine and isomeric pyridine groups play different roles in inducing RTP and responding to acid vapors, respectively. In CzS-*o*-py (1) and CzS-*p*-py (3), electron interactions and intermolecular charge transfer (CT) transitions were caused by tight molecular packing. In addition, intense intermolecular interactions induced persistent RTP features in these crystals with yellow phosphorescence emission. The phosphorescence quantum yield of CzS-*o*-py (1) was 15.36%. However, owing to its loose molecular arrangement with a low intersystem crossing (ISC) rate, CzS-*m*-py (2) emitted only blue fluorescence after 365-nm UV irradiation (**Figure 3C, D**). Different molecular packings lead to different photoluminescence behaviors. After fuming with hydrochloric acid vapor, they exhibited varied photoluminescence behaviors (**Figure 3E**). The yellow phosphorescence emissions of CzS-*o*-py (1) and CzS-*p*-py (3) turn to blue fluorescence and rare emission, respectively, while the blue fluorescence of CzS-*m*-py (2) changes to yellow fluorescence. This dynamic behavior results from molecular motion, which is attributed to the vibration of the phenothiazine group and the rotation of the pyridine substituent. After fuming with HCl vapor, the HCl molecule embedded into the dense crystal, wherein it combines with the nitrogen atoms of the pyridine group, thereby weakening the intermolecular interactions and intermolecular CT transitions. At the same time, the molecular

arrangement could recover its initial state after fuming with NH_3 vapor. Overall, the molecules need to move to search for another stable packing mode during the invasion of the HCl molecule.

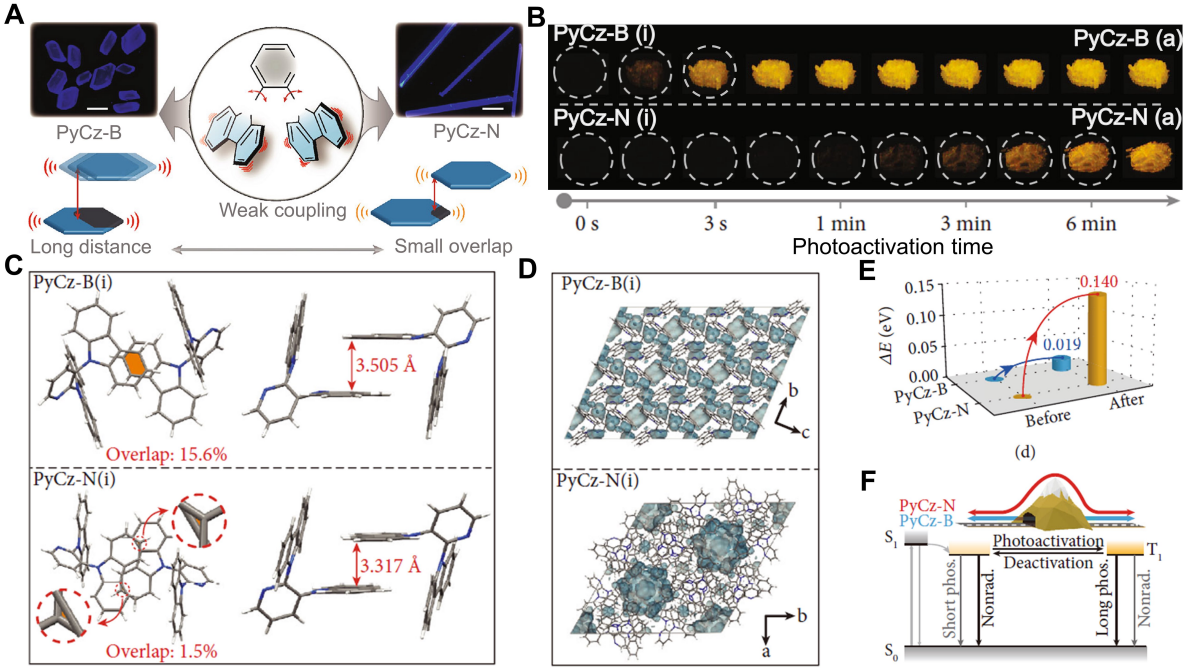

Figure 4. Polymorphs showing distinct responsive speeds under photoactivation.

(A) Structures of two polymorphs with distinct molecular packing modes. Insets show the fluorescence microscopy images (scale bar = 200 μm). (B) Phosphorescence photographs of PyCz-B and PyCz-N after photoactivation for different time periods (E_x = 365 nm, 40 mW/cm^2). (C) π–π overlap and distance of selected dimer with π–π interactions in PyCz-B (i) and PyCz-N (i). (D) Free volume region (cyan isosurface) in single crystal cells of PyCz-B (i) and PyCz-N (i). (E) Calculated change of single molecular energy of PyCz-B and PyCz-N before and after photoactivation. (F) Mechanism representation of polymorphs with distinct responsive speed after photoactivation. Reprinted with permission from Gu et al.[31] Copyright 2020 Exclusive Licensee Science and Technology Review Publishing House.

In addition to the aforementioned enhanced RTP strategies of molecular packing, the response and deactivation speeds of different molecular packing modes on the RTP performance are also worth exploring. In 2020, Gu et al. studied the dynamic ultralong organic phosphorescence of two polymorphs with different responsive features in detail.[31]

They cultured two polymorphs of PyCz, PyCz-B (block-type crystals) and PyCz-N (needle-like crystals), under different solvents. For PyCz-B, the lifetime prolongs from 44.52 to 868.86 ms after 3 s irradiation. However, PyCz-N needs photoactivation for 6 min to reach 776.03 ms of RTP from the initial 20.24 ms (**Figure 4A, B**). The response speed of PyCz-B was faster than that of the others because of three reasons. Firstly, the Å–Å distance of PyCz-B (3.505 Å) was longer than that of PyCz-N (3.317 Å) (**Figure 4C**). A longer π–π distance resulted in weaker π–π interactions. Thus, PyCz-B can move faster under photoactivation. Secondly, compared to the unoccupied space distribution of PyCz-N, PyCz-B exhibited more dispersed unoccupied spaces around the molecules (**Figure 4D**). Thus, the molecules in PyCz-B obtained more free space to adjust their configurations easily and reached the activated states in less time after photoactivation. Finally, the molecules reach a higher energy state as long as they overcome a large energy barrier (**Figure 4E, F**). Therefore, PyCz-B could be photoactivated more easily than the others. These three reasons demonstrate that different molecular stacking modes contribute to distinct responsive RTP features. In addition, the environmental atmosphere and irradiation intensity can influence the dynamic RTP behavior. Because of their unique ultralong organic phosphorescence characteristics, PyCz-B and PyCz-N were applied to a molecular logic gate.

Cross-linked bond-enhanced RTP

Use of poly(vinyl alcohol) (PVA) as a rigid matrix was reported in 2013 when Deng et al. obtained a carbon dot–PVA composite film with RTP by dispersing carbon dots in a PVA matrix.[32] The composite film was colorless and transparent under sunlight. The PVA matrix not only provides hydrogen bonds to solidify these carbonyl groups to effectively inhibit the nonradiative transition of triplet excitons but also plays an important role in preventing a direct collision between aromatic carbonyl units and oxygen molecules, a powerful RTP quencher, thus avoiding the quenching of RTP by oxygen. In recent years, PVA matrices have drawn increasing attention because it can provide a rigid environment for molecules to realize efficient and stable phosphorescence emission.

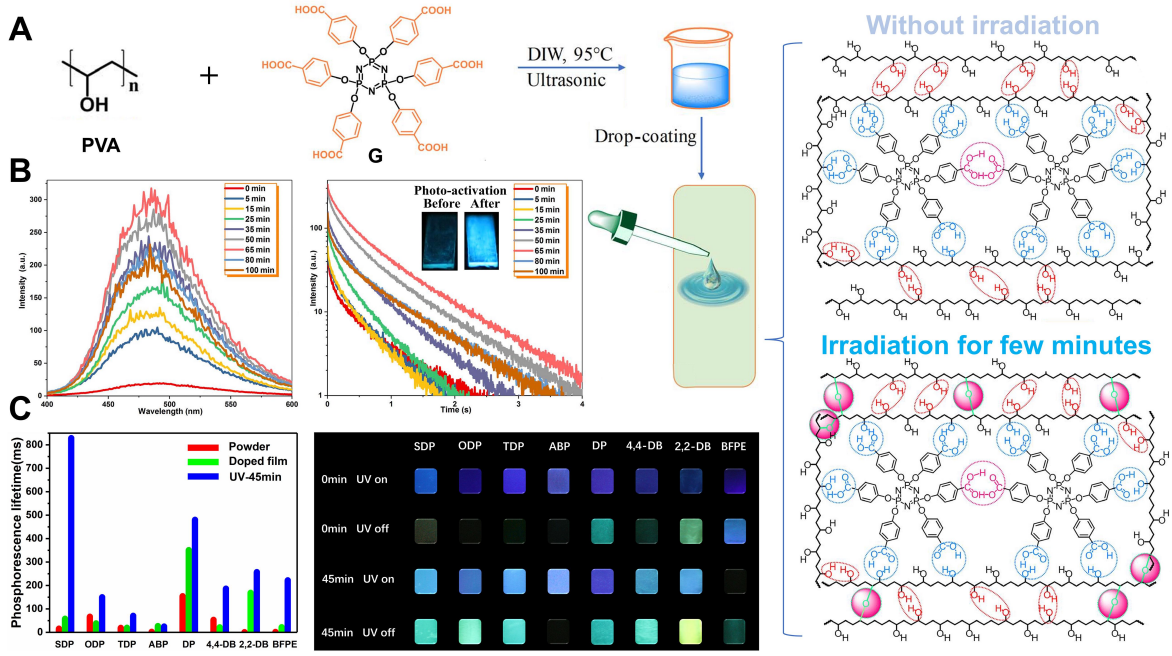

Figure 5. Irradiation-responsive behavior of PVA-based films.

(A) Preparation of irradiation-dependent film and the difference between irradiated and unirradiated internal structures. (B) Phosphorescence spectra and RTP-decay curves of the film under different 254-nm UV light irradiation times (λ_{ex} = 280 nm). Reprinted with permission from Su et al.[33] Copyright 2018 American Association for the Advancement of Science. (C) Intuitive lifetime comparison of eight different molecule-doped PVA systems under different conditions and fluorescence and phosphorescence images of eight different films with different irradiation times (λ_{ex} = 254 nm). Reprinted with permission from Zhang et al.[34] Copyright 2021 Springer Nature.

In 2018, we proposed a rational design to fabricate amorphous organic materials with ultralong RTP by introducing two types of intermolecular noncovalent hydrogen bonds and one type of covalent cross-linked bonds to PVA-based systems, which can inhibit the nonradiative transition of triplet excitation and further promote the ISC process from S_1 to T_1.[33] We designed an organic guest molecule containing six extended benzoic acid arms, i.e., hexa-(4-carboxy-phenoxy)-cyclotriphosphazene (G), which did not emit any visible fluorescence or phosphorescence under UV light at room temperature. A G-doped PVA film was obtained by doping G into the PVA matrix through simple physical embedding, followed by drip coating to form a film (**Figure 5A**). The G-doped PVA film showed blue-green RTP

after excitation by 254-nm UV light, with lifetimes and quantum yield of 0.28 s and 2.85%, respectively. This is due to the intermolecular (G-PVA) hydrogen bonds between the carboxyl groups of G and the hydroxyl groups of the PVA chain and intramolecular (G–G and PVA–PVA) hydrogen bonds. These bonds and the rigid PVA matrix inhibit the nonradiative transition of the molecules. Surprisingly, the RTP emissions of all G-doped PVA films irradiated with 254-nm UV light for 5–100 min were significantly enhanced. The film irradiated for 65 min was considered to be the most effective, and the corresponding RTP lifetime and quantum yield greatly increased to 0.71 s and 11.23%, respectively (**Figure 5B**). New cross-linkers (C–O–C) were formed between the PVA chains after irradiation, which further restricted the nonradiative transition of the system to improve the RTP efficiency. Thus, we developed a green screen-printing technique for the encryption and decryption of confidential information using the unique long-persistent emissions of these films. This is an interesting and efficient molecular design strategy for achieving large area and flexible RTP materials.

Inspired by this aspect, we have now gained more insight into the influence of irradiation on the photophysical properties of PVA systems in recent years. In 2021, our group proposed a design strategy for preparing a radiation-responsive RTP system through simple physical mixing of PVA and organic phosphors, without any complicated synthesis.[34] The selected organic molecules, (1,1′-biphenyl)-2,2′-dicarboxaldehyde (2,2-DB), bisphenol A (ABP), diphenyl sulfone (DP), 4,4′-oxydibenzaldehyde (BFPE), and 4,4′-sulfonyldiphenol (SDP), were used as phosphors incorporated into the PVA matrix, followed by drop-casting onto the glass substrate to form films. Because of the sufficient number of hydroxyl groups in the organic phosphors and PVA matrix, when the films were irradiated with UV light for 45 min, the hydroxyl groups in PVA activated to form oxygen radicals,[35] leading to the formation of cross-linked ether structures (C–O–C) with other hydroxyl groups in this system. Hence, all films exhibited excellent phosphorescence properties after irradiation. In particular, the dynamic phosphorescence lifetime of the SDP-doped film changed from 58.03 to 828.81 ms (14.3 times) and the phosphorescence quantum yield enhanced from 2.06% to 4.96% (2.4 times) (**Figure 5C**). Covalent bonding between PVA and the phosphors is not the only reason for the irradiation-enhanced phosphorescence emission. Molecular structure, hydrogen

bonding, and π–π stacking all play a positive role. Therefore, this study lays the foundation for the development of molecules with long-lived RTP and stimulus-responsive characteristics.

Oxygen-consumption-enhanced RTP

Usually, molecular oxygen presents a triplet ground state, which could interact with the triplet excitons of phosphors and quench their RTP emission. Thus, most examples of RTP were realized in the absence of oxygen. Inspired by this, dynamic RTP system based on the oxygen consumption mechanism under UV irradiation could be explored.[27] Poly(methyl methacrylate) (PMMA) has been reported as a good oxygen-consuming matrix.[36-38] Gmelch et al. reported an ultra-thin luminescent layer with a thickness of 900 nm using PMMA as a host and (*N*,*N*′-bis(1-naphthyl)-*N*,*N*′-diphenyl-(1,1′-biphenyl)-4,4′-diamine (NPB) as a guest, in which PMMA could inhibit the nonradiative transition of the triplet states.[37] In the absence of oxygen, the system exhibited long-lived RTP. This system was applied to various substrates, including transparent and flexible substrates. The top layer was covered with a 600-nm-thick oxygen barrier to avoid direct exposure of the luminescent layer to ambient oxygen. However, the sample fabricated under ambient conditions enabled the luminescent layer to contain molecular oxygen. When the sample (film) was irradiated with 365-nm UV light, the NPB molecule was excited and triplet excitons were formed through the ISC process. These triplet excitons are quickly quenched by molecular oxygen in the luminescent layer, resulting in ground-state NPB and excited singlet oxygen (**Figure 6A**). This singlet oxygen was consumed by the oxidation of PMMA. When the oxygen concentration was sufficiently low, phosphorescence was observed with the naked eye (**Figure 6B, C**). Because of these characteristics, the samples could be used to create programmable luminescent tags. The pattern information can be stored in the sample in the form of phosphorescence by irradiation through a mask or by direct use of UV laser spots (**Figure 6D**). The sample exhibited completely colorless transparency under visible light, and a clear phosphorescent image (>700 dpi) was obtained after the molecular oxygen in the sample was consumed by UV irradiation. The phosphorescent image could be easily erased by applying infrared light with a wavelength of approximately 4 μm for 1 min (**Figure 6E**). This was because, during the

heating process, the permeability of the oxygen barrier increased, so that the luminescent layer was filled with oxygen again, which led to the quenching of phosphorescence. This study represents a new approach for fabricating programmable illuminating tags that can replace traditional marking techniques.

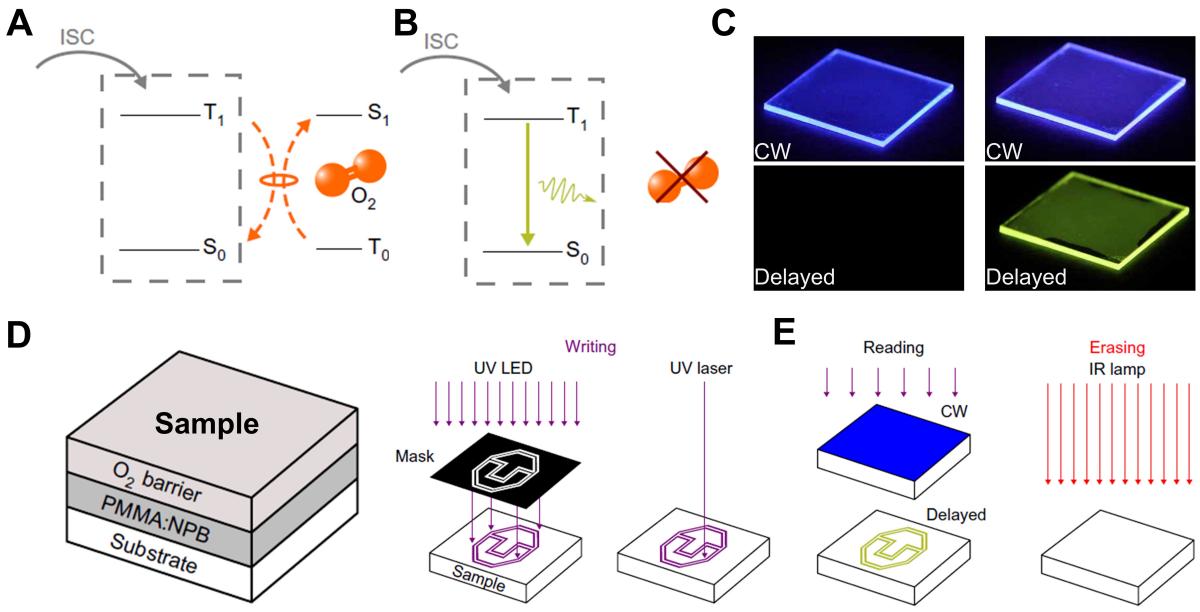

Figure 6. Erasable organic luminescent tags based on irradiation oxygen-consumption strategy.

(A) Triplet–triplet exchange between the T_1 state of NPB and molecular oxygen, accompanied by the generation of excited singlet oxygen. (B) NPB T_1 state slowly releases energy to return to the S_0 state in the absence of surrounding oxygen, generating phosphorescence. (C) Fluorescence and phosphorescence photographs of the presence (left) or absence (right) of oxygen in a PMMA matrix. (D) Irradiation oxygen depletion device and presentation of UV LED and linear laser writing strategies. (E) Readable mode based on irradiation-oxygen consumption strategy and infrared acceleration of oxygen into PMMA matrix for information erasure. Reprinted with permission from Gmelch et al.[37] Copyright 2019 Exclusive American Association for the Advancement of Science.

Inspired by this work, our group also applied this unique oxygen-consuming strategy to realize image display and multiple information encryption (**Figure 7A**).[38] Notably, the information exhibited was false under 365-nm UV light. However, after continuous UV light irradiation for approximately 60 s to consume the oxygen in the matrix, the pattern shows the

correct information “2021 PLPL” with green afterglow after removing the excitation source. This information is erased when oxygen enters the matrix. This erasable dynamic information encryption process is a feasible strategy for developing oxygen-consuming organic afterglow materials (**Figure 7B**).

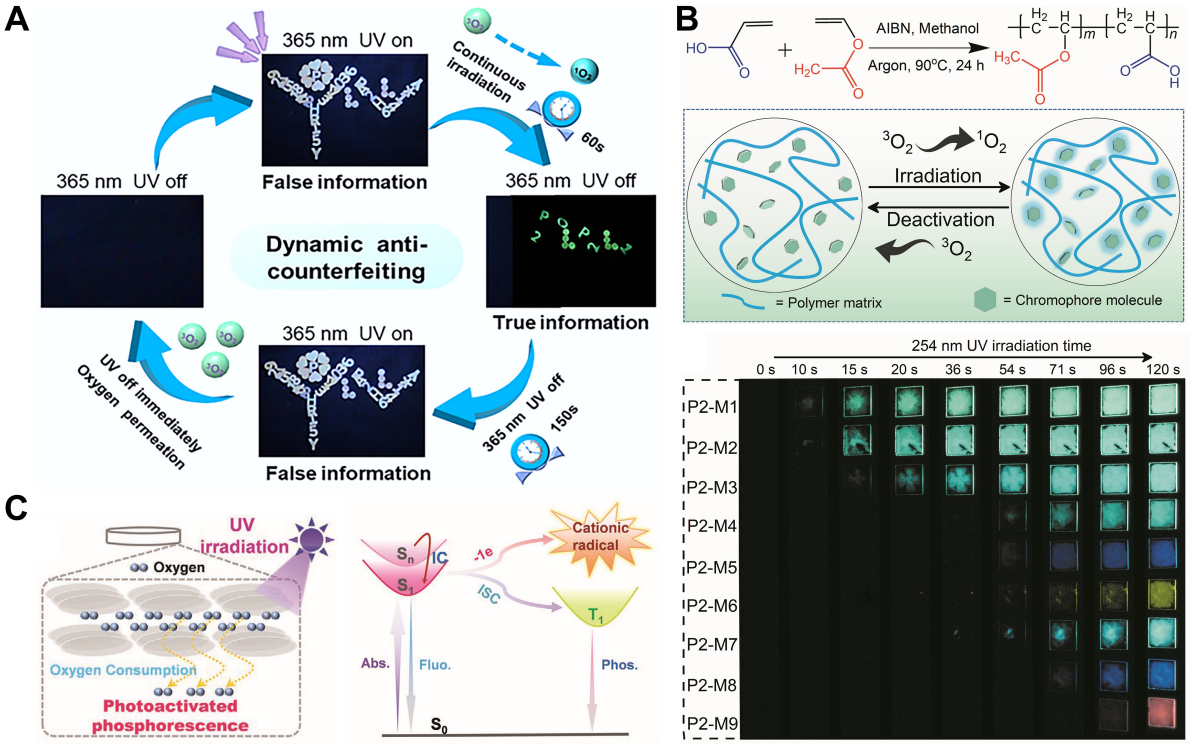

Figure 7. Tunable RTP property based on oxygen-consuming mechanism.

(A) Dynamic anti-counterfeiting applications of oxygen-consuming materials. Reprinted with permission from Wang et al.[38] Copyright 2022 Wiley-VCH GmbH. (B) Synthesis routes of the new oxygen-consuming substance and irradiation-oxygen consumption and deactivation process. Images show the RTP states of different films. Reprinted with permission from Wang et al.[43] Copyright 2021 Science China Press and Springer-Verlag GmbH Germany, part of Springer Nature. (C) Proposed mechanism for photoactivated phosphorescence and photochromic property. Reprinted with permission from Yang et al.[39] Copyright 2021 Wiley-VCH GmbH.

As a good oxygen-consuming matrix, PMMA has attracted great interest for the fabrication of luminescent materials. A series of triarylamine derivatives, synthesized by regulating conjugation, doped into PMMA films with photoactivated phosphorescence and photochromic properties were studied by Yang et al. (**Figure 7C**).[39] A film exhibited a

reversible photoactivated phosphorescence effect upon UV irradiation, resulting from oxygen consumption and efficient ISC transition of the triarylamine derivative. Owing to UV-induced electron transfer to form cationic radicals, the appearance of the films quickly changes from colorless to green under UV light and can be restored to the natural state in 15 min. Various applications and dynamic anti-counterfeiting and information encryption have been developed by utilizing the unique characteristics of PMMA.

The phenothiazine unit is a useful system to obtain RTP materials with excellent luminous properties because the N and S heteroatoms in phenothiazine prompt the n–π^* transition and ISC process.[27,40] Inspired by this, Wang et al. prepared a series of phenothiazine derivatives containing one, two, and three phenothiazine groups: 10-phenyl-10H-phenothiazine (PM-1), 1,4-di(10H-phenothiazin-10-yl)benzene (PM-2), and 1,3,5-tri(10H-phenothiazin-10-yl)benzene (PM-3), respectively. They were doped into the PMMA matrix to form luminescent films (**Figure 8A, B**).[39] All of them exhibited good RTP after UV irradiation for 30 s, even though no RTP was observed at the initial stage. After a series of characterization studies, they found that irradiation-dependent RTP resulted from oxygen consumption in the PMMA matrix. In the air, the presence of oxygen in the film is inevitable. Therefore, after UV excitation, the phenothiazine molecule was excited from the ground state (S_0) to the S_1 state and then to the T_1 state by ISC. Unfortunately, the presence of oxygen in the film quenched the triplet excitons by absorbing their energy, resulting in the absence of RTP. With uninterrupted UV irradiation for approximately 30 s, oxygen was almost completely converted from the initial triplet oxygen to singlet oxygen, which reacted with the sulfur moiety. Consequently, the triplet excitons decayed to the S_0 state, accompanied by a smooth phosphorescence emission. Owing to its unique oxygen-consumption properties, this material can be used to test the tightness of certain systems (**Figure 8C**). For example, an irradiated PM-3-P sample emitted RTP after storage for 19 d (without oxygen penetration). The PMMA polymer matrix, as an organic glass, is often used in aircraft windshields, furniture, architecture, and precision optical instruments.[41] However, PMMA materials may develop some microcracks after long-term use. Therefore, it is necessary to periodically check PMMA materials to avoid disasters caused by their fatigue fracture. Because the sample exhibited photo-induced RTP properties owing to oxygen consumption, a unique

microcrack-detection technology was developed. PMMA materials generally show two types of cracks: Form I and form II. The former is full of oxygen because of the presence of microcavities in it. PMMA materials doped with PM-3 do not exhibit RTP emissions in these cracked areas. In contrast, form II shows enhanced RTP emission because of internal refraction and reflection.[42] Under UV irradiation, the PMMA-doped materials exhibited three different phosphorescence emissions (**Figure 8D, E**). Cracks in the PMMA can be accurately and quickly identified using a gray-scale model. These samples are expected to be widely used in industrial and environmental applications.

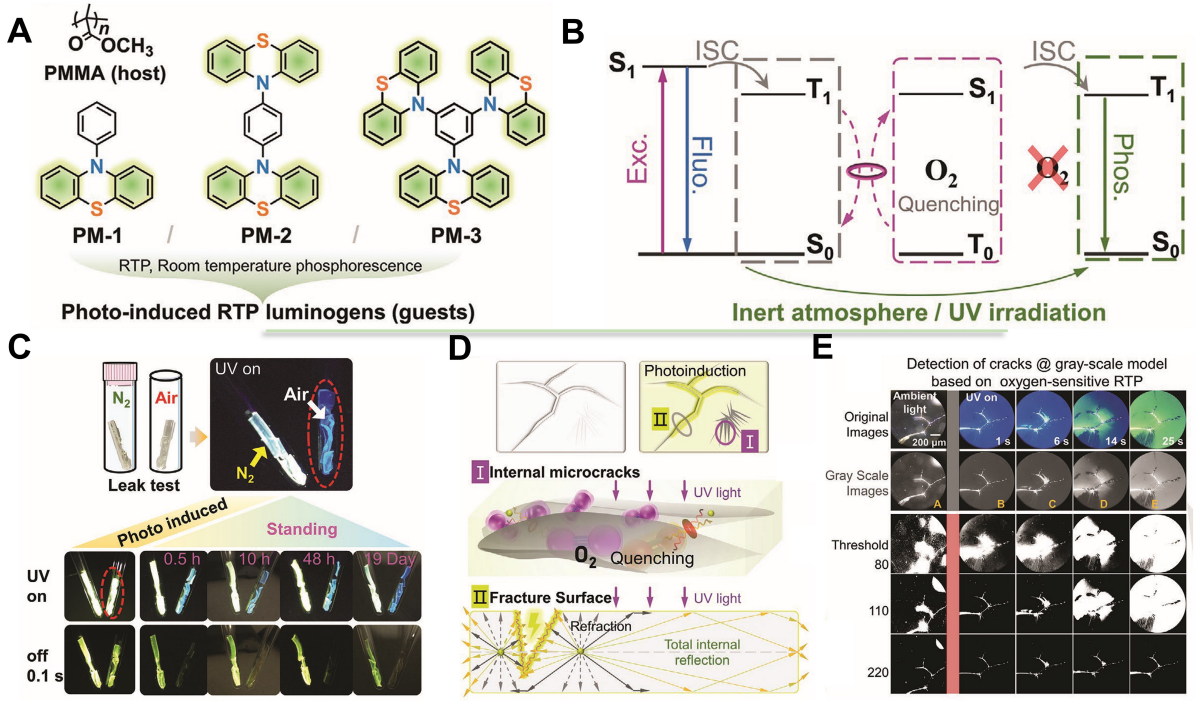

Figure 8. Airtightness and crack detection applications of PMMA-doped oxygen-depleting materials.

(A) Molecular structures of PMMA (host) and PM-1, PM-2, and PM-3 (guests). (B) Triplet exciton energy release pathway in the presence or absence of oxygen. (C) Air tightness detection: PM-3-P sample can keep the phosphorescence emission state in the nitrogen sealed after 19 days, and the phosphorescence phenomenon of another one fades away gradually in the air atmosphere. (D) Application of crack detection. (E) Images of gray-scale model based on oxygen-sensitive films. Different gray-scale level images were obtained using MATLAB. Reprinted with permission from Wang et al.[41] Copyright 2021 Wiley-VCH GmbH.

To date, most achieved RTP systems through oxygen consumption strategy are utilized PMMA as the matrix. To broaden the diversity of oxygen-consuming materials, it is important to develop new polymer matrices that can achieve excellent irradiation-dependent RTP. Our group recently proposed a general strategy by incorporating a series of organic chromophore molecules into a novel polymer matrix (P2–P9), prepared from vinyl acetate (VAc) and acrylic acid (AA) with different feeding ratios, to realize long-lived RTP with dynamic stimulus-responsive properties (**Figure 7B**).[43] We herein take the P2 (VAc:AA = 1:1)/4,4′-biphenol (M2) film as an example, which was made by doping M2 into P2 and drop-coating to form a film. Because the P2 polymer is full of -$COOCH_3$ groups with a low content of -COOH groups, the intermolecular hydrogen-bonding interaction between the P2 matrix and the M2 molecule is insufficient, which results in strong molecular vibrations. The unstable triplet exciton in the film is further quenched by triplet oxygen, causing an inability to achieve long-life RTP. However, after the film was irradiated with UV light for a few seconds, triplet oxygen converted to excited singlet oxygen. Thus, the phosphorescence intensity, lifetime, afterglow brightness, and quantum yield of the P2–M2 film increased by 155, 262, 414, and 8 times, respectively, compared to those of the pristine state. This irradiation-dependent RTP was attributed to the oxygen-consumption mechanism.

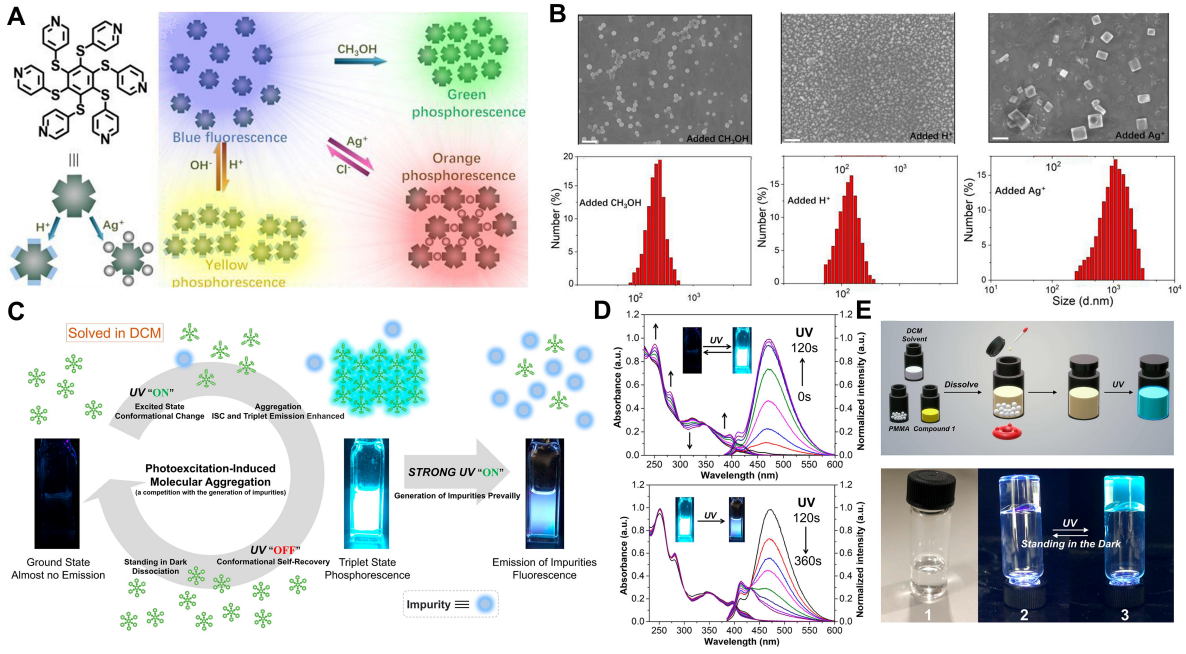

Figure 9. Dynamic phosphorescence properties obtained by manipulating molecular aggregation behavior through photoexcitation.

(A) Changes in the molecular aggregation state of HPTB under different additives. (B) SEM images and DLS results for HPTB assembly under the corresponding stimuli (CH_3OH, H^+, and Ag^+). Scale bar = 1 μm. Reprinted with permission from Jia et al.[52] Copyright 2020 Royal Society of Chemistry. (C) AIE and self-recovery behavior of compound **1** solved in DCM under photoexcitation. Compound **1** undergoes side reactions under photoexcitation to produce impurities. (D) Absorption and emission spectral changes of compound **1** at different irradiation times. (E) Preparation illustration of the organogel and the images in different states (1: original state, 2: original state under UV light, 3: photostationary state upon UV light irradiation). Reprinted with permission from Weng et al.[53] Copyright 2021 American Chemical Society.

Emerging strategies for enhanced RTP

Aggregation-induced emission (AIE) can efficiently overcome the conventional aggregation-induced quenching effect with efficient phosphorescent emission under condensed or constrained states.[44,45] At present, AIE effects are used as biological probes for specific chemical reactions.[46,47] However, photoactivated photophysical property changes based on the AIP effect are still rare. In 2018, Jia et al. proposed[48] a strategy for achieving dynamic reversible phosphorescence emission by utilizing the AIE effect of typical AIE systems in water, i.e., polysulfated benzene derivatives.[49-51] Compound **3**, a hexathiobenzene skeleton with six carboxylate groups, exhibited intense phosphorescence emission at 77 K or room temperature and no photoluminescence at room temperature in solution under 365-nm excitation. After irradiation for a few minutes, **3** emitted green phosphorescence due to AIE. Therefore, AIE plays a critical role in realizing the dynamic RTP from “off” to “on.” The TEM images show a difference in the nanometer size before and after irradiation. Before photoactivation, the particles were approximately 15 nm in diameter with good dispersion. After irradiation, the particle diameter increased to >200 nm in the aggregated state. The formation of aggregated morphologies in an aqueous solution is evident from the change in the nanometer diameter. To further study relevant changes in the molecules in aqueous solutions, the authors performed the corresponding theoretical calculations. Torsion C1−C2−S−C3 (torsion 1) between benzene side chains and sulfur atom linked to central benzene tuned

from 120° to 90° with changed conformation (from the ground state "GS" to the first excited state "ES1"). Because smaller torsion contributes to a more regular structure, it is difficult for water to mix with molecules in the ES1 conformation, resulting in easier aggregation. Furthermore, the equilibrium structure of GS exhibited a larger space between the side chains than that of ES1. The large space of the side chains could contain more water molecules, such that the molecules could aggregate easily with less water in the ES1. Thus, the smaller torsion, more regular structure, and less space of side chains facilitated the formation of an aggregated state under 365 nm UV irradiation in water. After removing the stimulation source, the conformation recovered back to the GS from ES1 with compound dissociation. Reversible aggregation and dissociation processes could be cycled at least 10^3 times. The large number of cycles endows them with broad application prospects.

Hereafter, another polysulfated benzene derivative, hexakis(pyridin-4-ylthio)benzene (HPTB), was designed in which six pyridine groups substituted six carboxylate groups with a polysulfated benzene core.[52] Similarly, HPTB exhibited AIE properties in DMF solution after adding external CH_3OH, H^+, and Ag^+ (**Figure 9A**). In DMF, HPTB dispersed in a solution with the blue fluorescence emission. After the addition of CH_3OH, H^+, and Ag^+, aggregation of varying degrees was observed, with phosphorescent emissions of different colors. After the addition of CH_3OH in DMF, when the relative concentration of CH_3OH is >40%, HPTB begins to gradually aggregate to form nanospheres with an average diameter of approximately 200 nm, resulting in green phosphorescence emission. H^+ and Ag^+ can react with pyridine groups to convert them into the hydrophilic pyridine cation and the HPTB-Ag coordination network, respectively (**Figure 9B**). Therefore, the formation of aggregates endowed HPTB with strong yellow and orange phosphorescence in DMF. This conversion was reversible upon the addition of OH^- and Cl^-.

Following the above work, extensive studies on photoactivated AIE luminogens in organic phase were carried out using compound **1**, a typical persulfurated aromatic molecule, as the AIE luminogen.[53] After irradiating compound **1** in a dichloromethane (DCM) solution with 365-nm UV light, a strong cyan phosphorescence emission was observed, accompanied by a new emission band at 470 nm. The photoactivation behavior was similar to that of compound **3** (above work) in water. However, the enhanced phosphorescence emission band

at 470 nm reached a peak after irradiation for 120 s and then gradually decreased and disappeared upon increasing the irradiation time, accompanied by an increased emission band at 410 nm (**Figure 9C, D**). The distinct behavior after irradiation for over 120 s was due to side reactions (impurities) caused by photooxidation in the organic phase. Impurities have a significant negative effect on the self-recovery ability of **1** after photoactivation in the organic phase. Therefore, it is important to suppress the generation of impurities. Fortunately, various studies have shown that the generation of impurities can be effectively reduced by controlling light intensity, dissolved oxygen, and solution polarity. Furthermore, an organogel was prepared using compound **1** in PMMA, which could overcome photooxidation to a great extent with a low concentration of dissolved oxygen and organic solvents in the gel (**Figure 9E**). Research progress in photoexcitation-controlled AIE systems is undoubtedly a significant step forward in the development of smart opto-functional materials.

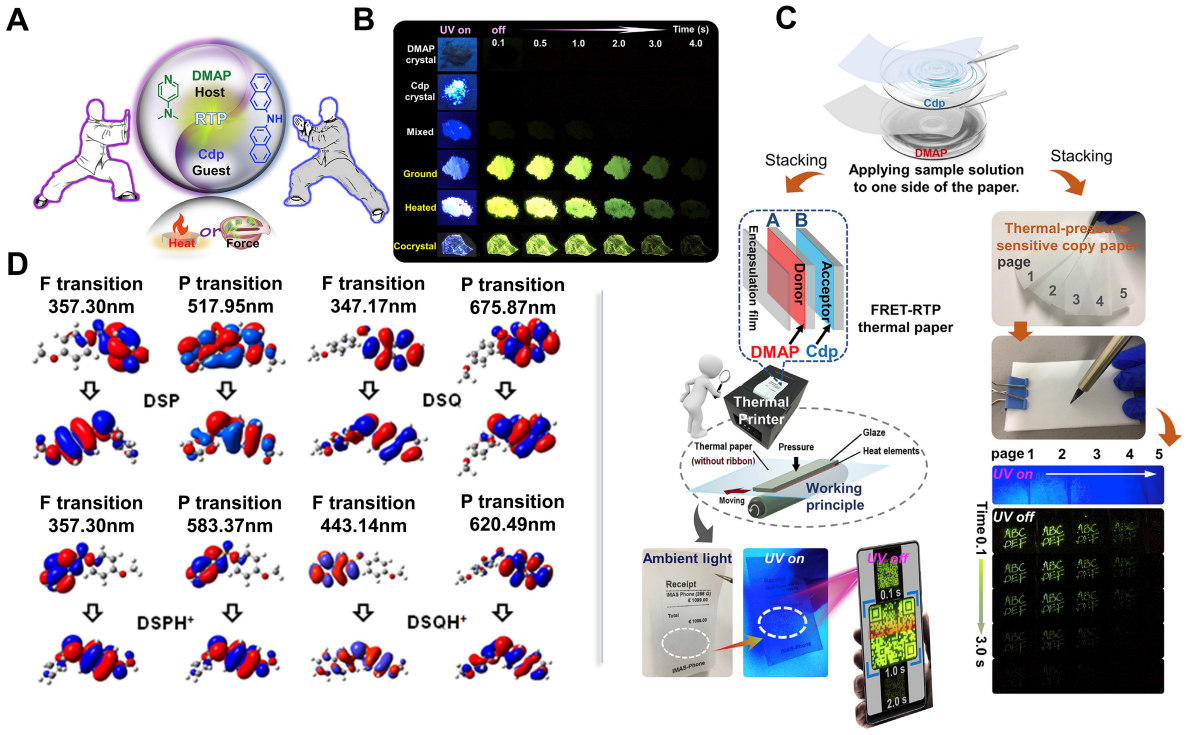

Figure 10. Dynamic RTP materials based on distance-sensitive FRET and charge transfer state between donor and acceptor.

(A) Design strategy diagram of distance-sensitive donor–acceptor system. (B) Fluorescence and phosphorescence photographs of DMAP and Cdp crystal and a mixed DMAP–Cdp sample under different conditions. (C) Application of thermal printing and thermo-pressure-sensitive copying paper. Reprinted with permission from Wang et al.[17]

Copyright 2020 Elsevier Inc. (D) Molecular orbital diagrams of DSP/$DSPH^+$ and DSQ/$DSQH^+$ pairs. Reprinted with permission from Huang et al.[59] Copyright 2018 Wiley-VCH Verlag GmbH & Co. KGaA, Weinheim.

In addition to utilizing the AIE effect to achieve dynamic RTP, the distance-sensitive Förster resonance energy transfer (FRET) process also can be utilized to promote dynamic RTP emission.[54] Only when the donor and acceptor are close enough that the electronic coupling can be produced and the excitation energy would transfer from the donor molecule to the acceptor molecules.[55,56] Wang et al. constructed a force-heating-responsive RTP system using the distance-sensitive FRET process (**Figure 10A**).[17] They selected *N*,*N*-dimethylpyridin-4-amine (DMAP) and di-(naphthalen-2-yl)-amine (Cdp) as the donor and acceptor, respectively. In DMAP, the presence of multiple nitrogen atoms supports the formation of intermolecular hydrogen bonds, which provide a rigid environment for the host–guest system. Cdp can emit RTP in a rigid matrix. In addition, their energy levels matched well, with a spectral overlap between guest absorption and host emissions. The above points are essential to realizing an effective dynamic RTP based on FRET. The DMAP and Cdp crystals alone did not emit phosphorescence at room temperature after the UV excitation was stopped. In addition, a simple physical mixture of DMAP and Cdp powders did not exhibit RTP. The DMAP–Cdp system exhibited bright green phosphorescence only for several seconds after grinding or heating (**Figure 10B**).

By utilizing Maxwell's electromagnetic theory to rationally explain force- or heat-responsive behavior, Förster used a donor as an electric field produced by an electrical oscillator. As long as the acceptor particles are close to the near-field of the donor particles propelled by an external force, energy is transferred from the interface layer of the donor to the acceptor.[57,58] Therefore, force and heat are the best thrusts to push acceptor particles into the near-field of the donor particle with FRET. With increasing heating or force, the DMAP emission at 334 nm decreased, and the fluorescence and phosphorescence emissions of Cdp at 405 and 500–600 nm were observed, respectively. The above spectral changes further indicate that RTP originates from the Cdp molecule and that DMAP inhibits the motion of the Cdp molecule. Inspired by distance-sensitive donor–acceptor system-based FRET, the authors

developed a thermo-pressure-sensitive copying paper to replace the conventional commercial thermal paper containing toxic bisphenol A. As shown in **Figure 10C**, the thermal paper was composed of a Cdp layer, a DMAP layer, and a transparent encapsulation film. The thermal paper contains a flexible isolation layer between the Cdp and DMAP that helps avoid direct contact between them. In addition, when Cdp was substituted by *N*-phenylnaph-thalen-2-amine (Cnp) as a guest molecule, the Cnp–DMAP system showed a similar dynamic RTP feature. This study demonstrated the generality of this strategy for designing stimuli-responsive RTP materials using distance-sensitive FRET.

To the best of our knowledge, most RTP-based sensors developed so far are "turn-off" types. Only small amounts of "off" to "on" RTP sensors are available in the liquid or liquefiable form at room temperature, which substantially limits their applications. Huang et al. reported a type of RTP "turn-on" sensor in solid state after exposure.[59] Sulfur was introduced as a bridging atom to connect the donor and acceptor moieties (DSA). To confirm the importance of the CT state between the donor and the acceptor, they designed two contrasting molecules, ASA and DSD. These two materials have only donor or acceptor parts. Among ASA, DSD, and DSA, only DSA exhibits strong yellow phosphorescence emission. To realize the "turn-on" sensor, two proton-activated acceptor substituents, pyridine (P) and quinoline (Q), were introduced to produce two sensing compounds, namely DSP and DSQ. The DSP and DSQ crystals were almost non-photoluminescent owing to the weak stacking interaction resulting from the highly twisted angle caused by the sulfur bond. Similar to DSA, DSP and DSQ exhibited bright yellow or green photoluminescence after acid-vapor treatment (with HCl and ArOH). Protonated $DSPH^+$ and $DSQH^+$ render RTP with a strong CT emission. Theoretical calculations were performed to further explore this mechanism (**Figure 10D**). Taking ASA and DSA as examples, for fluorescence (F) emission, the ASA F transition involves the entire molecule from the origin orbital to the destination orbital, whereas the DSA F transition occurs in one of the donor and acceptor regions, accompanied by a few overlaps. The phosphorescence (P) emission of ASA is similar to that of its F transition, whereas that of DSA is different. The origin orbital is localized on the acceptor moiety, whereas the entire molecule belongs to the destination orbital. Therefore, the extreme CT feature in the lowest singlet state transition renders DSA with a large ISC rate.[57,60] In DSP and

DSQ, the P emission exhibited a distinct difference before and after acid exposure, from the largely localized π–π* for P emission to strong CT transition. Therefore, the CT state played a critical role in enhancing the RTP properties of DSA, protonated $DSPH^+$, and $DSQH^+$. Thus, the "on" and "off" switching of RTP can be tuned by correspondingly changing a certain channel that turns the phosphorescence emission on, rather than only seeking a rigid matrix to suppress molecular vibrations.

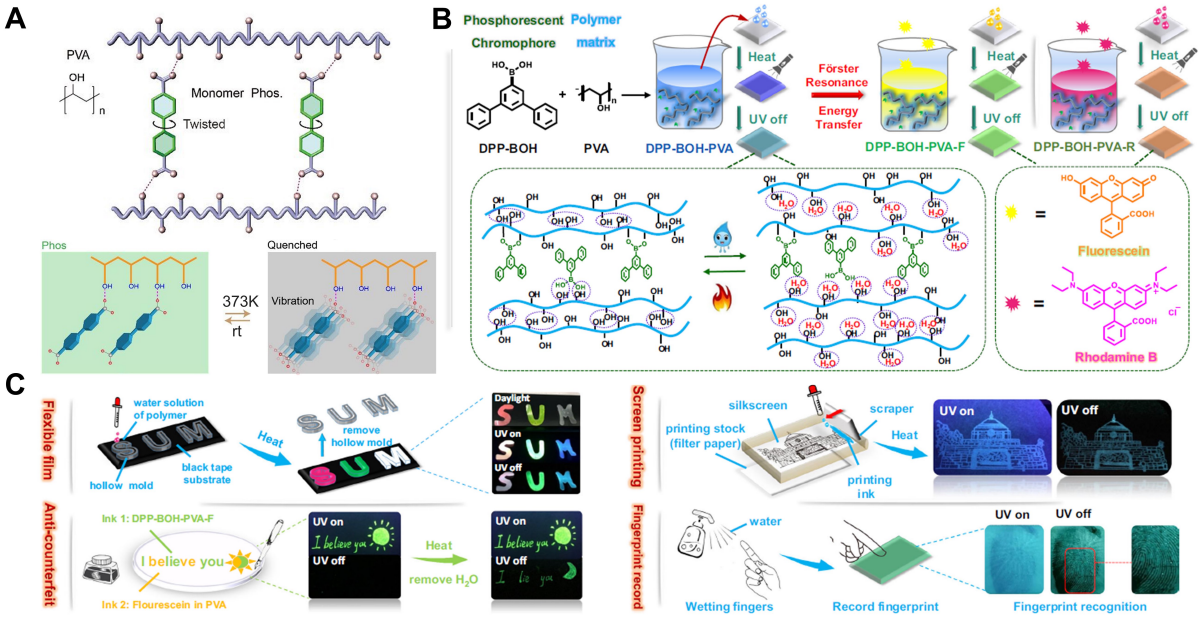

Figure 11. Tunable phosphorescence emission under water or high-temperature stimulus.

(A) Structure of co-assembly and schematic illustration of high-temperature-induced molecular vibrations leading to phosphorescence quenching. Reprinted with permission from Wu et al.[62] Copyright 2020 American Chemical Society. (B) Schematic diagram for the synthesis of three PVA-doped films and changes in intermolecular interactions under water or heating stimulus. (C) Applications of stimulus-responsive afterglow materials. Reprinted with permission from Li et al.[13] Copyright 2022 Springer Nature.

An elegant molecular design strategy for constructing stimuli-responsive RTP systems by combining the advantages of phosphorescence with supramolecular chemistry was developed.[61] Wu et al. prepared a phosphorescence system with reversible properties, which is highly sensitive to temperature changes and humidity in the air (**Figure 11A**).[62] Co-assemblies of PVA with biphenyl and naphthalene derivatives at low concentrations

afforded long-lived phosphorescence systems. However, excessive aggregation of organic molecules through intermolecular packing and hydrogen bonding interactions in films could completely depress their RTP emission. These small organic molecules exist in a monomeric state in the robust matrix provided by PVA at low concentrations, which is conducive to a strong ISC effect. In addition, the hydrogen-bonding interaction between them can inhibit molecular motion and collision. At high temperatures, the rigid matrix provided by PVA was unable to suppress strong molecular vibrations and rotations, which quenched the phosphorescence. In addition, the monomer state of the film makes the phosphorescence more sensitive to temperature. When the temperature returned to room temperature, the system was reversibly restored to its original state. Similarly, phosphorescence quenching originates from the breaking of the hydrogen-bonding network owing to interference by water molecules. The phosphorescence was recovered after drying the film for 2 min to remove water molecules. Based on the response to changes in temperature and humidity, it was concluded that this system could perform reversible switching in supramolecular networks.

Inspired by this strategy, Zhang et al. synthesized a series of room-temperature polymer phosphorescence materials with excellent photophysical properties. The maximum phosphorescence lifetime and maximum phosphorescence quantum yield of these materials can reach 369.88 ms and 14.36%, respectively.[63] The formation of strong mutual hydrogen bonding between vanilla derivatives and the PVA matrix effectively minimizes the nonradiative decay process, thereby generating long-life phosphorescent emission.[64,65] This system can maintain excellent luminescence properties under heating and cooling cycles between room temperature and 65 °C for up to 50 times, with good reversibility, which may help in the fabrication of long-lived luminescent polymeric materials. Li et al. also developed stimulus-responsive RTP materials under repeated stimulation with water and heating by using a PVA matrix (**Figure 11B**).[13] As seen in **Figure 11C**, four applications based on reversible phosphorescence features were realized.

CHANGE IN PHOSPHORESCENCE COLOR FROM BLUE TO RED

Color-adjustable luminescent materials have a wide range of applications as biomarkers, sensors, and flexible electronics as well as for anti-counterfeiting and biological detection

because of their unique photophysical features.[66-72] Some fluorescent materials with color-tunable emissions have been reported.[8,73] However, the development of color-tunable long-lived organic luminescence systems under ambient conditions has not been extensively studied.

Isolation-aggregation for color-tunable RTP

Carbon dots can change their phosphorescence emission color with different excitation wavelengths owing to the presence of multiple emitting centers.[74] Formation of multiple emission centers is the key to tunable emission color. Inspired by this phenomenon, Gu et al. designed a series of triazine derivatives with diverse heteroatoms, which not only exhibited efficient phosphorescence emission but also adjusted the emission color with varied excitation wavelengths.[75] They initially synthesized 2,4,6-trimethoxy-1,3,5-triazine (TMOT) to verify whether this speculation is reasonable. As expected, the emission color varied from sky blue to green under excitation wavelengths ranging from 250 to 400 nm; the emission peak also ranged from 452 to 505 nm. They analyzed different photophysical properties of TMOT dispersed in a dilute solution of 2-methyltetrahydrofuran (m-THF) or PMMA-encapsulated films at 77 K and reported that TMOT only exhibited blue phosphorescence emission at approximately 445 nm under 320-nm UV excitation in solution and that there were no emission peaks at other excitation wavelengths. The blue emission peak at 445 nm is similar to the emission peak at 452 nm in the TMOT crystal. Therefore, the blue emission at 452 nm can be attributed to the isolated molecular state, while the green RTP at 505 nm may originate from intermolecular aggregation in a single crystal. By viewing the arrangement of TMOT singlet crystals in the same plane along the b-axis, six TMOT molecules are connected by intermolecular interactions (C-H···N) to form a tight circle around the central molecule. Thus, each TMOT molecule can be tightly surrounded by molecular rings as a central molecule that suppresses the molecular motion and inhibits the nonradiative transition of triplet excitons. This limited molecular movement led to the formation of isolated molecules with blue phosphorescence emission. Observing from the a-axis perpendicular to the plane to see the adjacent parallel arrangement showed that the adjacent parallel presents face-to-face arrangement with H-aggregation by strong π–π interactions, bringing about stable green

ultralong organic phosphorescence emission. In addition, the 2,6-methoxy-4-diphenyl-1,3,5-triazin (MOPT) crystal (in which the methoxy group is replaced by a phenyl unit), which has a poor ability to suppress molecular motion in a plane, can only emit a yellow-green UOP, further indicating the importance of different molecular arrangement states for color tunability. Consequently, multiple intermolecular interactions in the same plane suppress molecular motion by forming isolated molecules with a blue emission, whereas face-to-face parallel H-aggregation induces molecular aggregation with green UOP. The tunable emission color of 2-chloro-4,6-dimethoxy-1,3,5-triazine and 1,3,5-triazinane-2,4,6-trione from violet to sky blue under various excitation wavelengths ranging from 250 to 400 nm proves the generality of this strategy. In addition, the phosphorescence lifetime and quantum yield can reach up to 2.45 s and 31.2%, respectively, because of the presence of several intermolecular interactions and a rigid crystal environment. Thus, this functional organic phosphorescent system with superior performance has promising application prospects.

Under ambient conditions, it is challenging to realize a color-tunable afterglow with a color range from blue to red using polymer systems. In 2020, our group prepared a series of polymer-based long-lived RTP materials with excitation dependence, which not only helped solve the issue of poor processing performance under environmental conditions but also addressed the problem of single and nonadjustable color.[76] A series of pyrene derivatives, 1-pyrenemethanol (PYM), 1-hydroxypyrene (HPY), 1-pyrenecarboxylic acid (PCA), and 1-pyrenylboronic acid (PBA), were doped into a robust PVA matrix and drop-cast to form films. The PVA matrix limits the nonradiative transitions of triplet excitons via hydrogen-bonding network formation. Two emission centers, one belonging to the isolated molecular state and the other to the aggregation state, occur simultaneously in the doped polymer matrix. Unlike the formation of isolated- and aggregated states in small-molecule crystals with varied molecular packing modes, the formation, in this case, was attributed to the movement of doped small molecules in the polymer matrix. Accordingly, on the basis of the experimental and theoretical investigations, we can conclude that the colorful polymeric RTP originates from the existence of isolated chromophores and aggregated chromophores, which can form different excited states. Under short-wavelength UV light (254 nm) excitation,

blue phosphorescence emission from the higher-excited-energy T_1 state was observed (**Figure 12A**). However, when excited by long-wavelength light (such as 365 nm), phosphorescence mainly originates from the lower-excited-energy T_1' state, showing a red afterglow. Thus, we successfully realized a tunable afterglow color from blue to red by varying the excitation wavelength **(Figure 12B)**.

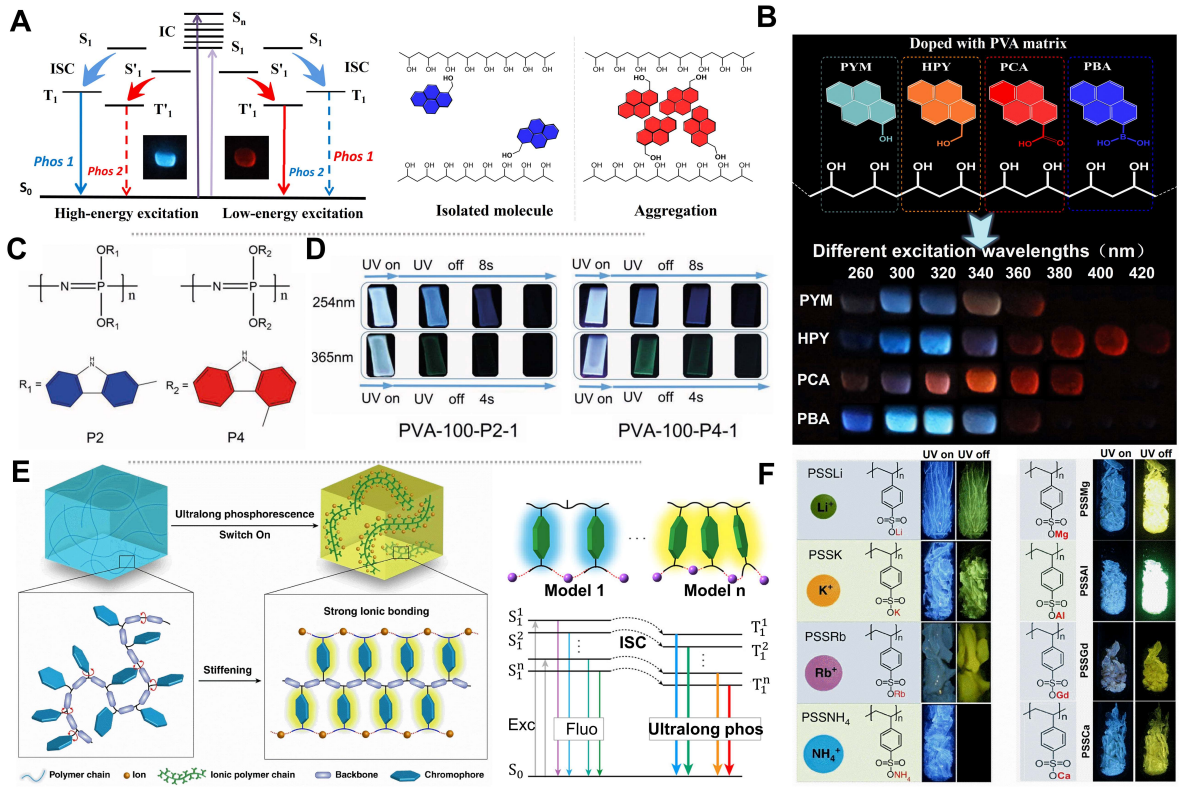

Figure 12. Excitation-dependent RTP polymers caused by isolation and aggregation states.

(A) Molecular schematic diagrams of isolation and aggregation states and the corresponding energy-level diagrams. (B) Chemical structures of PVA, PYM, HPY, PCA, and PBA, and the RTP images of their corresponding films exhibiting various colors at different excitation wavelengths. Reprinted with permission from Su et al.[76] Copyright 2020 Wiley-VCH Verlag GmbH & Co. KGaA, Weinheim. (C) Chemical structures of P2 (n = 9) and P4 (n = 7). (D) PLPL images of films under 254-nm and 365-nm UV light excitation. Reprinted with permission from Wang et al.[77] Copyright 2020 Wiley-VCH Verlag GmbH & Co. KGaA, Weinheim. (E) Schematic illustration for ultralong RTP in polymers supported by strong ionic bonds, and the proposed mechanism for excitation-dependence polymers. (F) Molecular

structure of polymers with different ion ligands and their corresponding fluorescence and RTP images (λ_{ex} = 365 nm). Reprinted with permission from Cai et al.[78] Copyright 2019 Springer Nature.

In order to further explore color-tunable polymeric RTP materials with longer phosphorescence lifetime, Wang et al. designed and synthesized novel excitation-dependent polymeric long-persistent luminescence (ED-PLPL) system by doping two polymer phosphors into PVA matrix.[77] They used 2-hydroxycarbazole (2-HC) and 4-hydroxycarbazole (4-HC) as raw materials, two polyphosphazene derivatives containing carbazole units, poly(2-hydroxyindazole phosphazene) (P2) and poly(4-hydroxyindazole phosphazene) (P4), were prepared (**Figure 12C,D**). These derivatives were then encapsulated in a robust PVA matrix to form films. The key factors for realizing stimulus-responsive ED-PLPL are the formation of hydrogen bonds and molecule-aggregated states. The hydrogen bonds among the polymer chains are easily destroyed by water absorption, although they can be restored by heating. Therefore, the ED-PLPL has broad prospects in the fields of information storage, display, anti-counterfeiting, and security encryption.

In addition to utilizing PVA as a rigid matrix, use of another type of suppressed environment has been reported by An et al.[78,79] by utilizing amorphous ionic polymers. Compared to hydrogen bonds, ionic bonds have the unique characteristics of strong interactions, non-directionality, and unsaturation. An et al. envisioned the possibility of introducing ionic bonds into the polymer, thereby suppressing the nonradiative transition of the chromophores to achieve long-lived RTP. To verify this hypothesis, amorphous poly(styrene sulfonic acid) sodium (PSSNa) was selected as the model ionic polymer. In this model, aromatic benzene rings act as chromophores, whereas sodium sulfonate substituents serve as chains that restrict the motion of the chromophores (**Figure 12E**). After the 365-nm UV excitation source was turned off at room temperature, yellow long-lived phosphorescence that lasted for several seconds under ambient conditions was observed by the naked eye. It was also found that as the excitation wavelength changed, the persistence luminescence exhibited a significant redshift, with the main peak changing from 540 to 560 nm and the corresponding lifetimes of 894 and 463 ms, respectively. The authors attributed such

significant differences in the phosphorescence lifetime to the different excited states produced by different aggregates between chromophores. At 77 K, the phosphorescence color change ranged from blue (λ_{em} = 441 nm) to orange (λ_{em} = 568 nm). When the temperature was increased to 443 K, the phosphorescence signal could still be detected from the PSSNa polymer owing to the strong interaction between the ions. In subsequent studies, different cations (Li^+, K^+, Rb^+, and NH_4^+) were used instead of Na^+ to obtain the corresponding ionic polymers. Similar to the PSSNa polymer, blue fluorescence and yellow long-lived phosphorescence were observed upon irradiation with a 365-nm UV lamp (**Figure 12F**). With an increase in the ionic radius, the RTP lifetime gradually decreased from 1308 ms (PSSLi) to 57 ms ($PSSNH_4$), which could be attributed to the quenching effect of heavy atoms or the weak nonradiative transition between benzene sulfonates. Additionally, the ionic polymers PSSMg, PSSCa, PSSAl, and PSSGd were synthesized using Mg^{2+}, Ca^{2+}, Al^{3+}, and Gd^{3+} ions, respectively. These polymers exhibit yellow (PSSMg, PSSCa, and PSSGd) or green long-lived phosphorescence (PSSAl). Notably, the PSSMg and PSSAl polymers possessed longer phosphorescence lifetimes than that shown by PSSNa, while the long-lived RTP lifetimes decreased from 1152 ms (PSSMg) to 845 ms (PSSCa) and from 765 ms (PSSAl) to 315 ms (PSSGd). They speculated that the highly charged ionic state was beneficial for prolonging the long-lived RTP lifetime, while a large ionic radius was not beneficial. Therefore, the long-lived RTP lifetime can be managed by balancing the ionic radius and charge state.

Changing emission intensity ratios for color-tunable RTP

Despite controlling the formation of isolated state and aggregated states to obtain long-lived organic luminescent materials with excitation dependence, researchers can still artificially introduce two different emission centers and adjust their phosphorescence intensity ratios under different stimuli (such as temperature and light) to obtain long-lived phosphorescent systems with adjustable colors. In 2020, Gu et al. presented a feasible strategy for achieving a distinctive color-tunable polymer-based UOP.[80] An excitation wavelength-responsive UOP systems can be obtained by conjugating multiple long-lived emission centers to the polymer backbone via radical crosslinking copolymerization. Owing

to hydrogen bonding between chromophore molecules and polyacrylic acid chains, the formation of a cross-linked polymer network provides a more rigid microenvironment for luminophores to restrict molecular motion and protect triplet excitons from quenching by oxygen or moisture from the external environment. The copolymer effectively emitted ultralong organic phosphorescence with a high quantum yield (37.5%). For instance, copolymer PDNA was synthesized through the radical cross-linked copolymerization of vinyl-functionalized naphthalene (MND), benzene (MDP), and AA (**Figure 13A**). The two luminophores in PDNA-MND and MDP-exhibited different phosphorescence emissions at the same excitation wavelength. The relative phosphorescent colors of MND and MDP are yellow and blue, respectively. The afterglow color of PDNA changed owing to different phosphorescence emission intensity ratios between the yellow phosphorescence of the MND monomer and the blue phosphorescence of the MDP monomer under variable excitation wavelengths. When the excitation wavelength was 230–302 nm, the blue luminescence intensity was stronger than that of the yellow one and the luminescence of the PDNA became blue. In contrast, when the yellow luminescence intensity was stronger than the blue one under 303–390-nm UV light, the PDNA exhibited yellow phosphorescence emission. Thus, different ratios of the phosphorescence emission intensities of benzene and naphthalene derivatives in PDNA allowed excitation-dependent color-tunable ultralong organic phosphorescence of multicomponent copolymers.

Similarly, inspired by this strategy, Zhang and coauthors realized the color-tunable phosphorescence emission of a supramolecular pseudopolyrotaxane polymer by utilizing the emission centers of benzene and naphthalene that exist simultaneously in the system.[81] In addition, 91 wt% NPR and 9 wt% diarylethylene (DAE) were combined using the photoisomerization properties of DAE derivatives.[82] Under 254-nm UV light irradiation, the closed DAE can transfer energy to NPR, resulting in the yellow-green phosphorescence quenching of NPR. Under visible-light irradiation, the DAE returns to the open state, the energy transfer ceases, and the NPR resumes phosphorescent emission. Thus, photo-controlled reversible polychromatic phosphorescence emission was achieved.

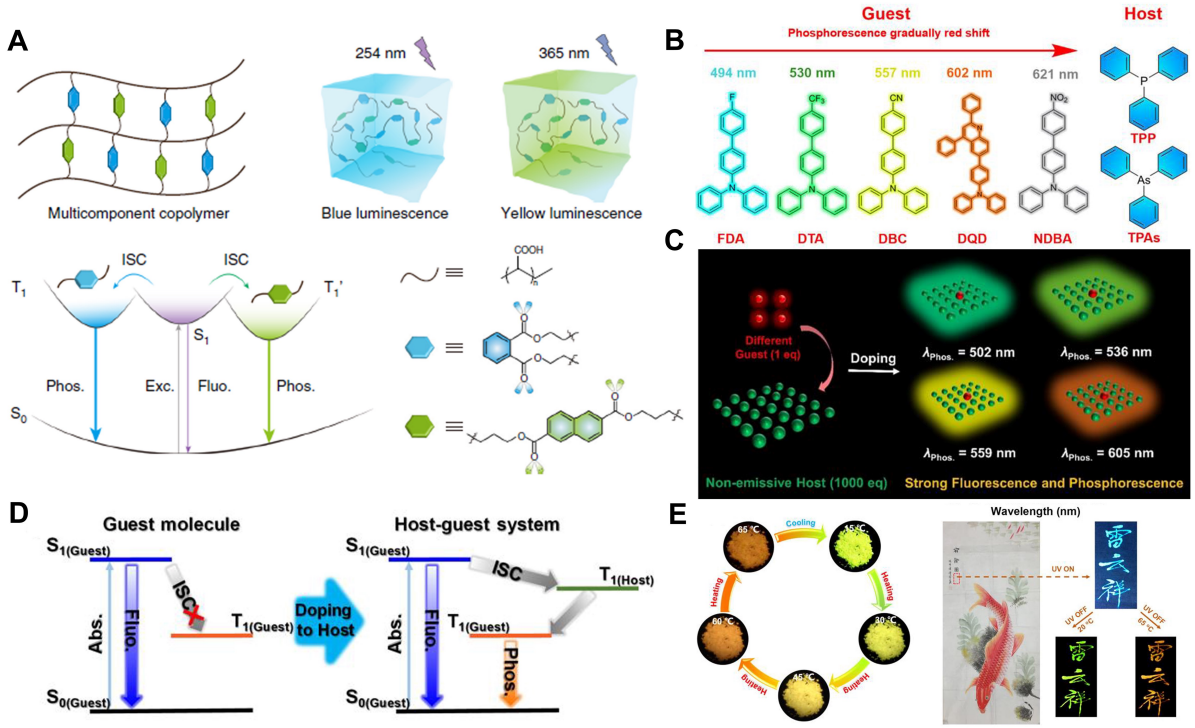

Figure 13. Color-tunable RTP materials by artificially introducing multiple emission centers.

(A) Schematic diagram of the strategy for cross-linking and copolymerizing chromophores with different emission centers to realize color-tunable RTP materials. Reprinted with permission from Gu et al.[80] Copyright 2020 Springer Nature. (B) Chemical structures of host and guest molecules. (C) Schematic illustration of host–guest interaction producing photoluminescence. (D) Energy-level analysis diagram for the interaction between host and guest materials. (E) Photographs of DTA–DQD/TPP host–guest system exhibiting varied colors at different temperatures and their corresponding application in anti-counterfeiting. Reprinted with permission from Lei et al.[83] Copyright 2020 Wiley-VCH Verlag GmbH & Co. KGaA, Weinheim.

At the same time, Lei et al. developed a series of host–guest organic phosphors with wide-ranging emission colors of phosphorescence from cyan to orange-red.[83] The host molecules play three important roles in this system: providing a rigid environment to suppress the molecular motion of guest molecules, protecting guest molecules from oxygen quenching, and assisting guest molecules to produce efficient phosphorescence emission. Therefore, triphenylphosphine (TPP) and triphenylarsine (TPA) were selected as host molecules because

of their highly stable subcooling states and low melting points (**Figure 13B**). Host–guest materials can be obtained by the melt-casting method with simple heating using hot water. Four guest molecules (FDA, DTA, DBC, and DQD) were dispersed in TPP and TPA to form eight host–guest systems with different phosphorescence properties. The phosphorescent color is mainly determined by the guest molecules; therefore, these eight host–guest systems exhibit phosphorescence emission colors ranging from cyan (502 nm) to orange-red (608 nm) with the phosphorescence lifetime and quantum yield tuning from 0.22 to 0.7 s and from 8% to 18%, respectively (**Figure 13C**). The four guest molecules could only emit phosphorescence at 77 K, owing to the low ISC rate from the large bandgap between S_1 and T_1. After interacting with host molecules, the host–guest systems exhibit high phosphorescence emission for the T_1 of the host molecule, acting as a bridge between S_1 and T_1 of the guest molecules to indirectly lower the bandgap and assist guest molecules in phosphorescence emission at a transitionary energy level (**Figure 13D**). The synergistic interaction of the host–guest system plays a crucial role in phosphorescence emission. Moreover, a three-component host–guest system, DTA-DQD/TPP (molar ratio = 1:1:1000), exhibited temperature-dependent phosphorescence with changeable colors based on the different degrees of phosphorescence intensity quenching when the temperature increased. For DTA/TPP and DQD/TPP, the emission peaks appeared at 536 and 605 nm, respectively. When the temperature increases to 65 °C from 15 °C, the phosphorescence intensities of DTA/TPP and DQD/TPP quench by 85% and 21% respectively, where different intensity attenuation can be attributed to different vibrational freedom in the system. In addition, the stronger electron-withdrawing ability of the DQD substituent than that of DTA results in an intense host–guest interaction in DQD/TPP compared to that in DTA/TPP, resulting in slower molecular vibration. Because the phosphorescence quantum yield of DTA/TPP is higher than that of DQD/TPP at 15 ℃, DTA-DQD/TPP exhibits green phosphorescence at 15 °C with the emission peak dominating at 536 nm. At 65 °C, the emission color changes to orange with a higher emission intensity at 605 nm. The phosphorescence color red-shifted from green to orange owing to different degrees of decrease in the phosphorescence intensity of DTA/TPP and DQD/TPP. Furthermore, it can recover the initial green phosphorescence after heating–cooling cycles, rendering the systems with applicable values. Because of the low melting

point of TPP, the systems can be easily heated to a molten state and poured into a brush for writing (**Figure 13E**). Thus, this method opens up new possibilities for generating dynamic RTP materials.

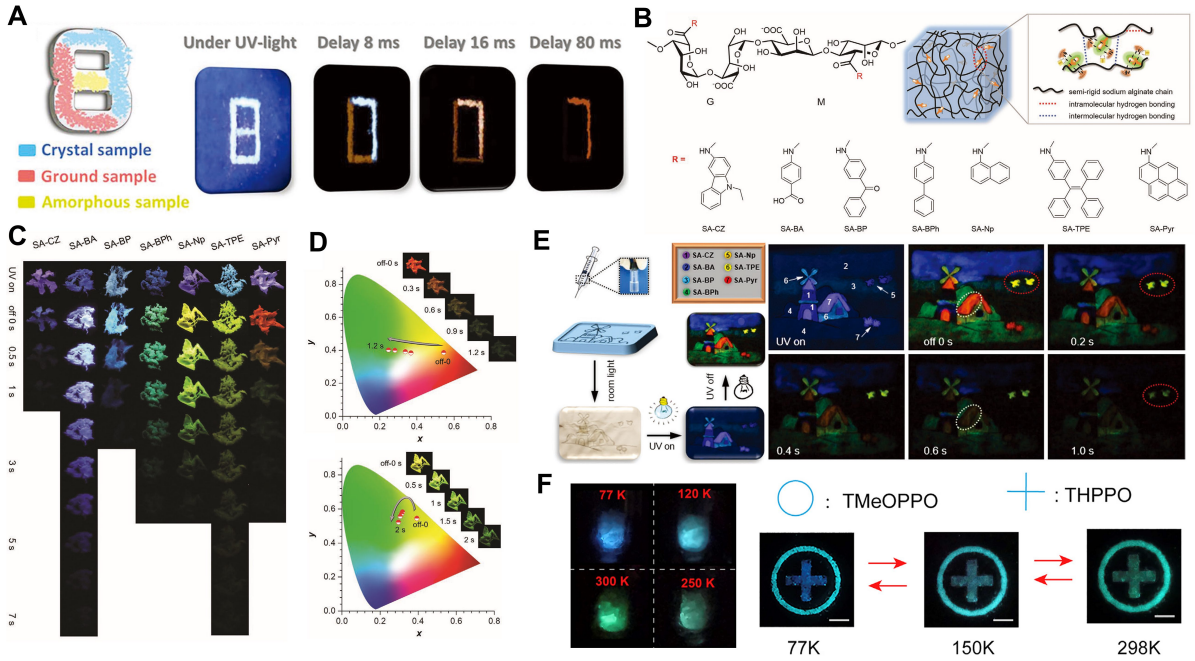

Figure 14. Schematic diagram of time- and temperature-dependent afterglow materials. (A) Pattern "8" composed of different aggregation states of SOBF-OMe and the corresponding images of afterglow decay at different times. Reprinted with permission from Chen et al.[84] Copyright 2019 Wiley-VCH Verlag GmbH & Co. KGaA, Weinheim. (B) Chemical structures of SA derivatives. (C) Fluorescence and RTP images of SA derivatives. (D) Time-dependent CIE coordinate locus plots of afterglow color for SA-Np and SA-Pyr solids. The inset images show the corresponding solid afterglows color with varied durations. (E) Patterns consisting of seven SA derivatives with different RTP colors for anti-counterfeiting applications (λ_{ex} = 312 nm). Reprinted with permission from Dou et al.[86] Copyright 2020 Wiley-VCH GmbH. (F) Images of temperature-dependent crystals exhibiting different phosphorescence colors at various temperatures. Reprinted with permission from She et al.[91] Copyright 2021.

For excitation- or temperature-dependent organic phosphorescent materials, the afterglow color can only change when the external stimuli change. In general, time-dependent afterglow materials are more convenient and intuitive, with the phosphorescence colors varying over

time. In 2019, Chi et al. used a molecule (SOBF-OMe) by bridging dibenzofuran moieties with weak intermolecular hydrogen bonds to obtain a single-component material that exhibits dual-emissive RTP, thermally activated delayed fluorescence (TADF), and time-dependent color-tunable afterglow (**Figure 14A**).[84] The time-dependent afterglow originated from the different decay lifetimes for TADF and RTP emissions. Since then, various time-dependent organic crystals based on different RTP and TADF decay rates have been reported.[85]

In contrast to the same emission species (dual emission of RTP and TADF) with different lifetimes, Dou et al. reported several sodium alginate (SA) derivatives with time-dependent persistent RTP (p-RTP) based on diverse p-RTP emissive species with different decay lifetimes.[86] Owing to several intramolecular hydrogen bonds formed in the SA matrix and the semirigidity of the SA chain itself, the SA polymer matrix can minimize the nonradiative transition of triplet excitons and protect the chromophore from oxygen or water quenching. Hence, the authors grafted a series of amine-containing molecules onto SA chains through amidation to obtain seven SA derivatives with afterglow colors varying from blue to orange-red (**Figure 14B, C**). Their phosphorescence lifetimes and quantum yields reached up to 1039 ms and 7.6%, respectively. Using multiple intra- and intermolecular molecular interactions, chromophores located inside the chains can form isolated monomers, dimer-like aggregates, and clusters with different energy levels and effective conjugation lengths, which can induce a color-tunable afterglow when the excitation wavelength is changed. Surprisingly, SA-Np and SA-Pyr exhibited time-dependent RTP. The time-dependent afterglow was ascribed to distinct emissive species from clusters with different lifetimes. SA-Np demonstrated three emission peaks—505, 542, and 580 nm—with lifetimes of 450, 577, and 423 ms, respectively. When the excitation ceased, the three emission peaks were emitted together with yellow phosphorescence. With time, the RTP color changed to greenish-yellow and finally green, with a sequential decay of the emission peak intensity at 580, 505, and 542 nm (**Figure 14D**). Similarly, the RTP color of SA-Pyr varied from red to orange-red, orange-yellow, yellowish-green, and finally green, with different decay lifetimes of the emission peaks (516, 616, 667, and 730 nm). Consequently, the different intensity decay ratios of the various emission peaks dominated the phosphorescence colors over time. Benefiting from tunable color by changing the excitation wavelength and time as well as the

good film-forming ability and water solubility, this system can be used for anti-counterfeiting and multi-coding data encryption (**Figure 14E**). Inspired by this aspect, in 2021, Miao et al. reported a color-tunable ultralong RTP crystal based on melamine (MEL) with excitation- and time-dependent properties.[87] Inexpensive and organic phosphorescent MEL can change the RTP color from blue to green with varying durations and excitation wavelengths, which is ascribed to the different lifetime and intensity ratios between the molecular phosphorescence and the ultralong phosphorescence from H-aggregation. Temperature-responsive RTP systems for anti-counterfeiting and visual temperature detection will be discussed in **Figure 14F**.

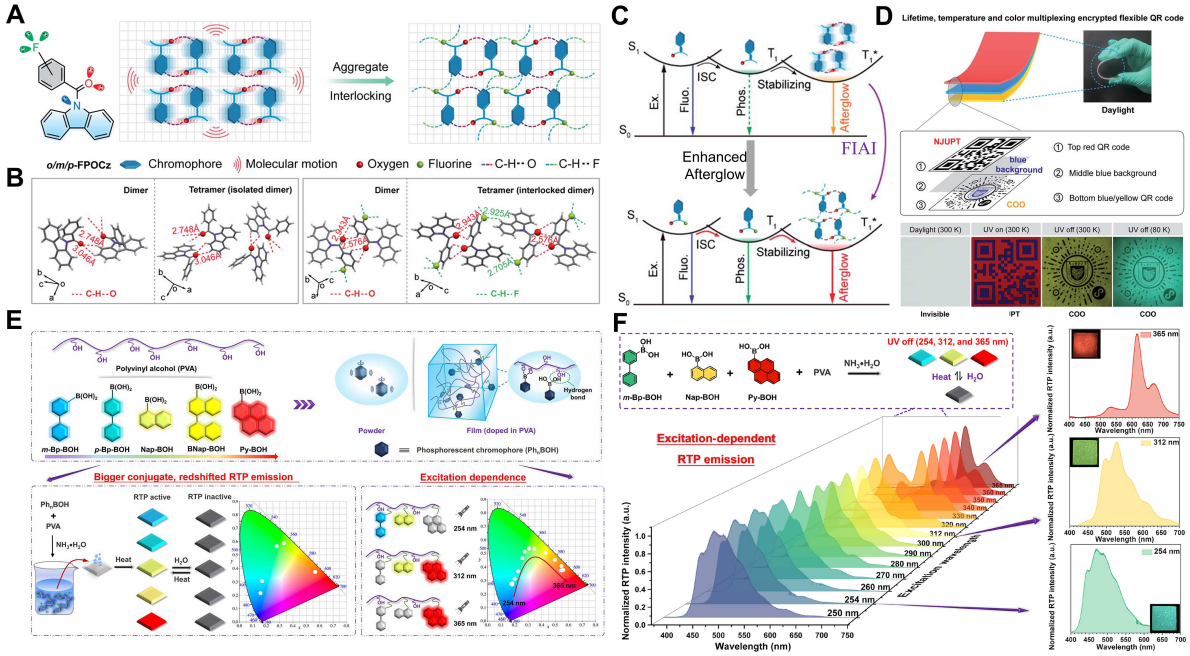

Figure 15. Color-tunable afterglow materials with different emission intensity ratios under different conditions.

(A) Chemical structure of *o*/*m*/*p*-FPOCz and schematic illustration of the FIAI strategy. (B) Intermolecular interactions of the dimer and tetramer (left: POCz single crystal, right: m-POCz single crystal). (C) Schematic illustration of the mechanism for enhancing organic afterglow performance by FIAI. (D) 3D encryption application based on temperature, lifetime, and color. Reprinted with permission from Li et al.[90] Copyright 2021 Royal Society of Chemistry. (E) Stimulus-responsive excitation-dependent RTP system. (F) Preparation route of doped PVA film and the emission peaks of phosphorescence spectra at different excitation wavelengths showing a redshift trend. Reprinted with permission from Li et al.[16] Copyright 2022 Exclusive American Association for the Advancement of Science.

As everyone knows, for RTP materials, the phosphorescence quantum yield (Φ_p) and lifetime (τ_p) are innate contradictions because the efficient ISC rate (K_{ISC}) and low nonradiative decay rate ($K_{nr}^{T^*}$) are incompatible in the same system. This problem must be solved to obtain high-brightness and long-lived organic afterglow materials. Thus, a few studies about simultaneously improving K_{ISC} and $K_{nr}^{T^*}$ have been reported.[88,89] Li et al. proposed fluorine-induced aggregate interlocking (FIAI) to realize both enhanced quantum yields and prolonged lifetime.[90] Unexpectedly, the fluorine-containing molecules exhibit temperature-dependent afterglow. They introduced a fluorine atom into a POCz compound at different positions on the benzene ring to obtain three isomers: *o*-, *m*-, and *p*-FPOCz (**Figure 15A**). To better illustrate the key role of the fluorine atom, POCz was used as a blank control molecule. In terms of the ISC rate, the singlet and triplet splitting energies (ΔE_{ST}) of *o*/*m*/*p*-POCz (ΔE_{ST} < 0.37 eV) are lower than those of POCz. The SOC values of *o*/*m*/*p*-POCz (>0.3 cm^{-1}) are larger than those of POCz. The efficient ISC channel numbers of *o*/*m*/*p*-POCz were 3, 5, and 4, respectively, whereas the channel number was only 2 for POCz. These results indicate that, after introducing the fluorine atom, the K_{ISC} greatly improved from 1.32×10^6 s^{-1} of POCz to 5.84×10^7 s^{-1} of m-POCz, which is approximately 54-fold larger than POCz. The shorter fluorescence lifetime of *o*/*m*/*p*-FPOCz than that of POCz further illustrates the enhancement in the ISC rate. For nonradiative decay rates, the authors performed a detailed comparison of the single-crystal structure and theoretical analysis. The dimers of POCz crystals demonstrated only one type of intermolecular interaction (C-H···O). All dimers can vibrate freely because of the absence of any noncovalent interactions among them, resulting in poor afterglow properties. In contrast, there are not only intermolecular interactions (C-H···O) within dimers but also intermolecular interactions (C-H···F) between the neighboring dimers of *o*/*m*/*p*-FPOCz. Hence, the abundant intermolecular interactions in the dimers and adjacent dimers promote molecular interlocking and suppress nonradiative decay, endowing *o*/*m*/*p*-FPOCz with a superior afterglow performance (**Figure 15B, C**). In addition, H-aggregation was observed in the *o*/*m*/*p*-FPOCz single crystals to further minimize the nonradiative decay rates. Consequently, the enhanced K_{ISC} and decreased $K_{nr}^{T^*}$ simultaneously render *o*/*m*/*p*-FPOCz with high efficiency (Φ_p = 10.5%) and long lifetime

($\tau_p = 1.09s$). The unexpected temperature-dependent afterglow feature can be attributed to dual phosphorescence emission with different intensity-increasing ratios. When the temperature decreased from 300 to 80 K, the intensity of the initial emission peak at 527 nm from the aggregated T_1^* increased. Interestingly, a new emission peak emerged at approximately 460 nm upon decreasing the temperature. Owing to the different ratios at 460 and 527 nm, the corresponding Commission Internationale de L'Eclairage (CIE) coordinates range from (0.36,0.59) to (0.24,0.40) as the temperature decreases from 300 to 80 K. Using the afterglow features and temperature-dependent characteristics obtained via the FIAI strategy, a tri-mode multiplexing encryption with a quick response (lifetime, temperature, and color response) was developed. The three layers exhibit different photophysical phenomena under different stimuli (**Figure 15D**). Thus, the FIAI strategy can be used to obtain good afterglow materials with high quantum yields and long lifetimes.

The color-tunable RTP materials with temperature dependence are scarce now. In 2021, She et al. reported temperature-responsive phosphorescent crystals with a color change from blue to green upon increasing the temperature from 80 to 300 K.[91] Different substituent groups induced distinct photoactive behavior in these crystals. This distinct responsive behavior can be attributed to different molecular packing modes and intermolecular interactions. A temperature-dependent color-tunable phenomenon was observed only in the crystal (THPPO). At room temperature, two main emission peaks at 467 and 494 nm were observed in the phosphorescence spectra of THPPO. A new emission band emerged at 426 nm when the temperature decreased to 257 K. The strongest emission peaks changed from 467 and 494 nm at 300 K to 426 nm at 80 K, resulting in phosphorescence colors ranging from green to blue with wide CIE coordinates from (0.17,0.17) to (0.21,0.44). A new peak at 426 nm appears because the cryogenic temperature induces a more rigid environment with slower molecular motion for enhanced T_1 phosphorescence.[92] Given the photo- and temperature-responsive RTP features, they can be used for anti-counterfeiting and visual temperature detection (**Figure 14F**). More recently, Li et al also reported an RTP system based on an amorphous PVA polymer doped with a series of arylboronic acids for full-color tunability and achieved information encryption with Morse code and screen printing (**Figure 15E, F**).[16]

Different internal states of molecules for color-tunable RTP

For organic small-molecule-based phosphorescent systems, ultralong organic phosphorescence is usually obtained by constructing a rigid environment with a low nonradiative decay rate. To date, a robust environment has mainly been provided by crystals with multiple intermolecular interactions and metal-organic frameworks (MOFs) with effective coordination bonds. Hence, there is an urgent need to develop additional systems to enrich the family of organic phosphorescent materials. Cheng et al. reported a type of organic ionic crystal with multiple UOP colors.[8] This ionic crystal can be obtained through ionic bonding in water owing to its good solubility in ammonia solution. In this case, terephthalic acid (TPA) can be converted to transparent block ammonium hydrogen terephthalate (AHT) crystals upon evaporation. The presence of ammonium cations facilitates a face-to-face arrangement of adjacent TPA chromophores, resulting in shorter distances for intermolecular interactions with more stable H-aggregation, which greatly promotes the generation of UOP. In addition, ionic bonds connecting terephthalate anions and ammonium cations slow down the molecular vibrations and motions and effectively lock the conformation of the terephthalate anion. Therefore, AHT exhibited green phosphorescence emission lasting several seconds after the 365-nm excitation light source was removed (**Figure 16A**). To verify the applicability of the ionic crystal environment, they prepared two additional ICs: dipotassium terephthalate (DPT) and disodium terephthalate (DST). As expected, DPT and DST exhibited different ultralong organic phosphorescence colors, sky blue and yellow-green, with lifetimes of 504 and 585 ms, respectively. The three distinct ionic crystals with UOP demonstrated the critical role of ions in promoting phosphorescence generation. In addition, the presence of ions endowed AHT with color-tunable phosphorescence under alternating ammonia and hydrogen chloride gas fuming. TPA powder without ammonium cations exhibited yellow phosphorescence. After fuming the TPA powder with ammonia gas for several minutes, it was transferred to the AHT salt comprising a combination of terephthalate anions and ammonium cations. Thus, the ultralong organic phosphorescence color changed from yellow to blue-green, with a blue shift of the main emission peak from 520 to 506 nm and a weakened emission band at 390 nm with increasing fuming time. Surprisingly, the

phosphorescence color returned to the initial stage after decomposing AHT to TPA and NH_4Cl under hydrogen chloride gas fumigation for 7 h (**Figure 16B**). The color change from yellow to green and then back to yellow was repeated more than four times.

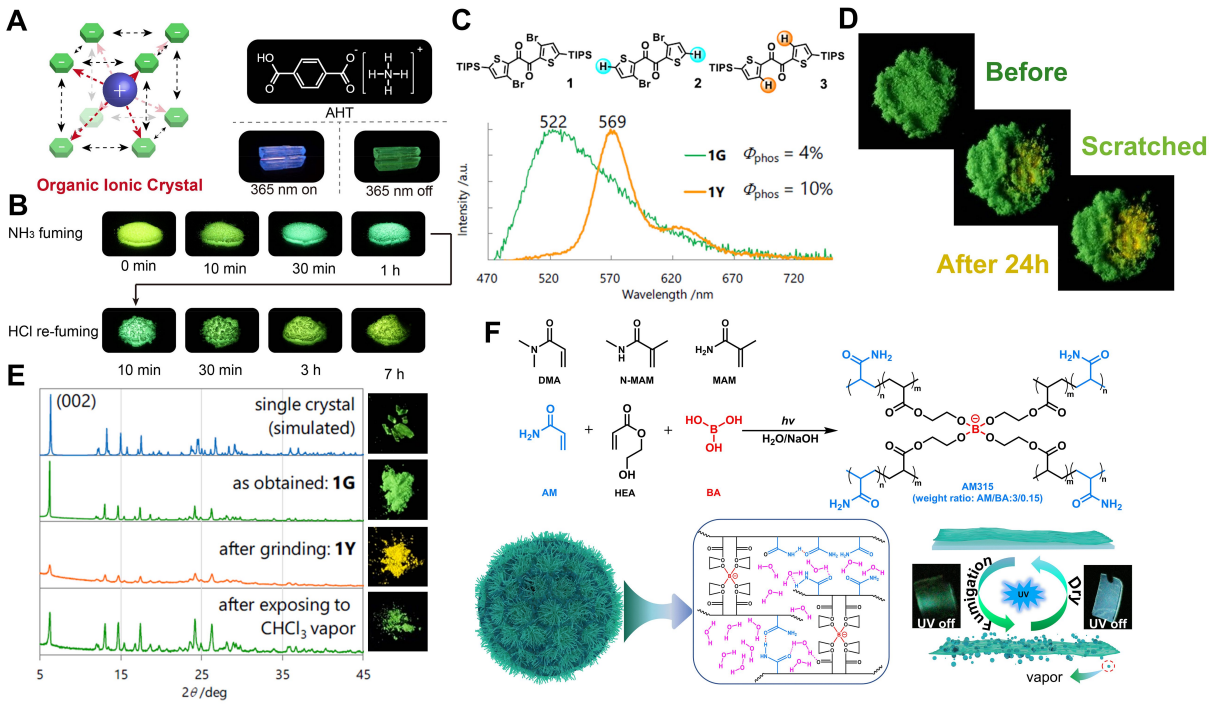

Figure 16. Color-tunable afterglow materials based on different states within molecules. (A) Representation of an organic ionic crystal for ultralong organic phosphorescence and the chemical structure and images of AHT crystal before and after excitation (λ_{ex} = 365 nm). (B) Phosphorescence images of the materials under NH_3 and HCl fuming. Reprinted with permission from Cheng et al.[8] Copyright 2017 Wiley-VCH Verlag GmbH & Co. KGaA, Weinheim. (C) Chemical structures of thenil derivatives **1**–**3** and the solid-state photoluminescent spectra of **1**G and **1**Y. (D) Slow self-recovering behavior of derivative **1** under ambient conditions and room temperature. (E) Powder X-ray diffraction profiles of single crystals of **1** (simulated), **1**Y, **1**G, and **1**Y after exposure to $CHCl_3$ vapor. Images show their phosphorescence state after excitation at 365 nm. Reprinted with permission from Tani et al.[93] Copyright 2019 Royal Society of Chemistry. (F) Synthesis routes of copolymer AM315 and the corresponding stimulus-responsive behavior under water and dry conditions. Reprinted with permission from Gao et al.[98] Copyright 2021 Wiley-VCH GmbH.

Crystallization is a useful method for achieving ultralong organic phosphorescence

because an ordered molecular arrangement and multiple intermolecular interactions can effectively suppress the nonradiative transition of triplet excitons. Therefore, destruction of the lattice usually weakens the phosphorescence intensity or even quenches it. In 2019, Tian et al. reported an unusual color-tunable RTP system based on a crystal-to-amorphous phase transition.[93] Thenil **1** was synthesized from 2-bromothiophene. Compound **1**G was obtained by the recrystallization of thenil **1** from a mixed $CHCl_3$/methanol solution, which emitted green phosphorescence similar to that exhibited by **1**. After grinding the crystalline powder **1**G, **1**Y were obtained. Interestingly, **1**Y exhibited distinct yellow phosphorescence at approximately 569 nm and an enhanced quantum yield from 4% to 10% (**Figure 16C, D**). Powder X-ray diffraction patterns revealed sharp diffraction peaks of **1**G and broadened weak peaks of **1**Y, which demonstrated crystal conversion to an amorphous state under grinding (**Figure 16E**). To explore the mechanism of the color change and the improvement in the phosphorescence quantum yield after amorphization, structural analysis and theoretical calculations were conducted. The experimental data indicated that a small part of the trans-planar conformation appeared upon grinding **1**Y, which was the main source of yellow phosphorescence. The original green phosphorescent moiety from the skew conformer decays to the ground state through a thermally activated nonradiative decay pathway in such a loose environment.[94] In general, trans-planar confirmation is not metastable in the ground state because of its lack of bistability. Chalcogen bonding in **1** rendered the trans-planar conformer metastable to emit yellow phosphorescence with high efficiency. Subsequently, the authors synthesized thenil derivatives **2** and **3**. Thenil **2** bearing H substituents showed non-phosphorescence emission in the solid state. The difference between **3** and **1** is that **3** does not contain Br atoms or chalcogen bonds. Hence, thenil **3** with RTP did not show changeable colors after grinding. Consequently, stabilizing the trans-planar conformation of chalcogen bonds and having suitable substituent groups for molecular arrangement are essential for realizing efficient RTP and color-tunable features. Thenil **1** shows slow self-recovery to the initial crystal state after heating, exposure to $CHCl_3$ vapor, or exposure to room temperature for 24 h. Its recovery mechanism may involve recrystallization using the remaining crystals.[95]

Generally, polymeric RTP materials with longer luminescence lifetimes can only perform

stable phosphorescent emission in a safe environment without quenchers (e.g., water, oxygen, and high temperature), because the presence of these species causes the quenching of triplet excitons. To date, there have been only a few reports on phosphorescence systems in the aqueous environment.[48,96,97] Recently, Gao et al. reported an amorphous RTP system with high luminescence performance, showing color tuning from blue to green by water.[98] Different from the conjugated structure of conventional luminescence systems, they utilized click chemistry to synthesize nonconventional luminescent polymers. As shown in **Figure 16F**, because of the presence of hydrogen bonds and cross-linked networks, molecular rotation and movement were strictly restricted and nonradiative transitions were inhibited. The afterglow lifetime and phosphorescence quantum yield are up to 841.06 ms and 10.48%, respectively. The afterglow color of the RTP system was blue under 287-nm UV light excitation and dry conditions. Surprisingly, after a few minutes of fumigation with water vapor, the phosphorescence was not quenched; instead, a green afterglow was observed under 287-nm excitation. After fumigation, the water adsorbed inside the polymer connects the hydrogen bond interactions between the components,[86,99] thereby forming large cross-linked networks that decrease the energy of the triplet state from 2.78 to 2.64 eV and render the emission redshift with the phosphorescence color range from blue to green. This work not only expands the application range of amorphous RTP materials but also lays down the foundation for developing water-induced smart systems with adjustable colors.

CONCLUSIONS AND OUTLOOK

We systematically reviewed the latest research progress on dynamic organic RTP materials from the perspectives of phosphorescence intensity and color. Various organic RTP systems with stimuli-responsive characteristics are classified in terms of emission intensity and color, based on their different forms of response to external stimuli (such as light, force, temperature, and vapor). Changeable inter/intramolecular interactions, molecular structure, conformation, formation of cross-linked bonds, and consumption of oxygen in the matrix are responsible for the phosphorescence intensity demonstrated by responsive phosphorescent systems. Isolated and aggregated states are the main factor responsible for the emission color exhibited by excitation-dependent RTP materials. Furthermore, the emission intensity ratios

from the same or different emission species can vary based on changes in temperature, time, and excitation wavelength, resulting in distinct colors of organic RTP materials. The presence of cations, the amorphization of crystals, and the invasion of water molecules also endow RTP materials with color-tunable capabilities. Thus, four types of responsive modes, that is, structural diversification, changes in interaction or distance among molecules, formation and dissociation of bonds between molecules, and changes in the oxygen content around molecules, are responsible for the distinct responsive behavior of organic RTP materials. Light is an intuitive, external stimulus. After excitation by light with various irradiation durations and wavelengths, RTP systems can directly exhibit responsive luminescence without any physical contact. Force-, temperature-, and vapor-responsive RTP materials have promising application prospects. Undoubtedly, more research on dynamic organic RTP materials will open up new avenues for further development in this important field.

Despite promising research progress on dynamic organic RTP materials, a series of challenges remain. (1) The key to improving the phosphorescence quantum yield of dynamic RTP lies in the fast radiation transition rate, slow non-radiation transition rate, and fast ISC efficiency; however, a rapid radiation transition rate decreases the phosphorescent lifetime. Therefore, the high phosphorescence quantum yield and long phosphorescence lifetime are inherent contradictions, and it is difficult to improve them simultaneously. Fortunately, some strategies such as supramolecular self-assembly, free volume modulation, and resonance-activated spin flipping might be simultaneously improved quantum yields and prolonged lifetimes. (2) The triplet excitons generated through the ISC process are extremely unstable. Hence, a feasible strategy is required to stabilize them. Some previous work demonstrated that moderate improvement of the rigid environment in the material system can effectively stabilize the triplet excitons, and the introduction of carboxylic acids, carbazoles, and other groups can also effectively enhance the ISC process.[33,75,89,92] (3) At present, the stimulus source of dynamic RTP materials is often a single stimulus. The phosphorescence properties of materials under external stimuli show little change, especially the phosphorescence intensity. The development of dynamic RTP materials that can efficiently enhance their response and phosphorescence properties to multiple stimuli remains a problem worth exploring. We proposed that introducing multiple functional groups with

stimulus-response sites into the same system could achieve multiple stimulus source responsiveness. (4) The applications of dynamic organic phosphorescent materials are limited by the fact that the materials usually have poor mechanical properties and are easily affected by quenchers. Thus, new application directions should be developed to meet the ever-changing scientific and technological society. Comfortingly, some unique RTP materials have been reported. For example, Wu et al. obtained a water-resistant RTP material, which can still emit bright phosphorescence after being soaked in water for 12 weeks.[96] Cai and co-workers prepared organic phosphorescent materials in the form of high mechanical strength foams.[100] Ma and co-workers reported an organic fluid phosphorescence system.[61] These progresses represent the development of dynamic RTP materials with better performance, indicative of the bright future of RTP materials. (5) Compared with molecular crystals, amorphous RTP materials with good processability would better meet the increasingly complex and demanding requirements. Nevertheless, further development of polymeric RTP materials is still needed, due to the low availability of polymer matrix. The exploration of more novel polymer matrices is highly necessary. (6) To date, the dynamic RTP materials are mainly excited by UV light. The excitation sources such as near infrared light, visible light, and X-ray should be used to develop dynamic RTP materials.

For dynamic RTP systems, their RTP behaviors (emission color, intensity, and lifetime) could demonstrate dynamic change under external stimuli, such as light, heat, mechanical force, and so on. Compared with static RTP systems, the dynamic RTP effect presents much more potential practical applications due to their good reversibility, quick response and easy to control. These above-mentioned aspects are both challenges and opportunities, and naturally indicate the future development directions of dynamic organic RTP systems. For further development of dynamic RTP systems, AI should be accurately used to promote molecular design with effectively dynamic RTP performance with the rapid development of AI. We believe that the prospects of dynamic organic RTP materials are bright, and their properties and performance will be significantly expanded for practical applications.

ACKNOWLEDGMENTS

This work was financially supported by the National Natural Science Foundation of China

(22275025 and 21875025), the Innovation Research Group at Institutions of Higher Education in Chongqing (CXQT19027), the Graduate Research and Innovation Project of Chongqing (CYS21442), the Chongqing Talent Program, the Science and Technology Project of Banan District, the Innovation Support Plan for the Returned Overseas of Chongqing (cx2020052), the Open Fund of Guangdong Provincial Key Laboratory of Luminescence from Molecular Aggregates (2021-kllma-03), and the Agency for Science, Technology and Research (A*STAR) Singapore through Its Manufacturing, Trade and Connectivity (MTC) Individual Research Grant (M22K2c0077).

AUTHOR CONTRIBUTIONS

Qian Zhou: Conceptualization, Writing-original draft. Chaolong Yang: Conceptualization, Writing-review & editing, Funding acquisition, Supervision. Yanli Zhao: Writing-review & editing, Funding acquisition.

DECLARATION OF INTERESTS

The authors declare no competing interests.

References

1. Fermi, A., Bergamini, G., Roy, M., Gingras, M., and Ceroni, P. (2014). Turn-on phosphorescence by metal coordination to a multivalent terpyridine ligand: A new paradigm for luminescent sensors. *J. Am. Chem. Soc. 136*, 6395-6400.

2. Zhen, X., Tao, Y., An, Z., Chen, P., Xu, C. Chen, R., Huang, W., and Pu, K. (2017). Ultralong phosphorescence of water-soluble organic nanoparticles for in vivo afterglow imaging. *Adv. Mater. 29*, 1606665.

3. Hirata, S., Totani, K., Yamashita, T., Adachi, C., and Vacha, M. (2014). Large reverse saturable absorption under weak continuous incoherent light. *Nat. Mater. 13*, 938-946.

4. Kabe, R., Notsuka, N., Yoshida, K., and Adachi, C. (2016). Afterglow organic light-emitting diode. *Adv. Mater. 28*, 655-660.

5. Rumsey, W. L., Vanderkooi, J. M., and Wilson, D. F. (1988). Imaging of phosphorescence: A novel method for measuring oxygen distribution in perfused tissue. *Science 41*, 1649-1651.

6. Dolmans, D. E. J. G. J., Fukumura, D., and Jain, R. K. (2003). Photodynamic therapy for cancer. *Nat. Rev. Cancer 3*, 380-387.

7. Xie, Z., Zhang, X., Wang, H., Huang, C., Sun, H., Dong, M., Ji, L., An, Z., Yu, T., and Huang, W. (2021). Wide-range lifetime-tunable and responsive ultralong organic phosphorescence multi-host/guest system. *Nat. Commun. 12*, 3522.

8. Cheng, Z., Shi, H., Ma, H., Bian, L., Wu, Q., Gu, L., Cai, S., Wang, X., Xiong, W. W., An, Z., et al. (2018). Ultralong phosphorescence from organic ionic crystals under ambient conditions. *Angew. Chem. Int. Ed. 57*, 678-682.

9. Yang, Z., Xu, C., Li, W., Mao, Z., Ge, X., Huang, Q., Deng, H., Zhao, J., Gu, F. L., Zhang, Y., et al. (2020). Boosting the quantum efficiency of ultralong organic phosphorescence up to 52% via intramolecular halogen bonding. *Angew. Chem. Int. Ed. 59*, 17451-17455.

10. Yan, Z.-A., Lin, X., Sun, S., Ma, X., and Tian, H. (2021). Activating room-temperature phosphorescence of organic luminophores via external heavy-atom effect and rigidity of ionic polymer matrix. *Angew. Chem. Int. Ed. 60*, 19735-19739.

11. Xu, W.-W., Chen, Y., Lu, Y. -L., Qin, Y. -X., Zhang, H., Xu, X., and Liu, Y. (2021). Tunable second-level room-temperature phosphorescence of solid supramolecules between acrylamide–phenylpyridium copolymers and cucurbit[7]uril. *Angew. Chem. Int. Ed. 61*, e202115265.

12. Yang, J., Fang, M, and Li, Z. (2021). Stimulus-responsive room temperature phosphorescence materials: internal mechanism, design strategy, and potential application. *Acc. Mater. Res. 2*, 644-654.

13. Li, D., Yang, Y., Yang, J., Fang, M., Tang, B. Z., and Li, Z. (2022). Completely aqueous processable stimulus responsive organic room temperature phosphorescence materials with tunable afterglow color. *Nat. Commun. 13*, 347.

14. Huang, Q., Mei, X., Xie, Z., Wu, D., Yang, S., Gong, W., Chi, Z., Li, Z., and Ling, Q. (2019). Photo-induced phosphorescence and mechanoluminescence switching in a simple purely organic molecule. *J. Mater. Chem. C 7*, 2530-2534.

15. Yang, Y., Liang, Y., Zheng, Y., Li, J. -A., Wu, S., Zhang, H., Huang, T., Luo, S., Liu, C., Shi, G., et al. (2022). Efficient and color-tunable dual-mode afterglow from large-area and flexible polymer-based transparent films for anti-counterfeiting and information encryption. *Angew. Chem. Int. Ed. 61*, e202201820.

16. Li, D., Yang, J., Fang, M., Tang, B. Z., and Li, Z. (2022). Stimulus-responsive room temperature

phosphorescence materials with full-color tunability from pure organic amorphous polymers. *Sci. Adv. 8*, abl8392.

17. Wang, Y., Yang, J., Fang, M., Yu, Y., Zou, B., Wang, L., Tian, Y., Cheng, J., Tang, B. Z., and Li, Z. (2020). Förster resonance energy transfer: An efficient way to develop stimulus-responsive room-temperature phosphorescence materials and their applications. *Matter 3*, 449-463.

18. Wang, C., Gong, Y., Yuan, W., Zhang, Y. (2016). Crystallization-induced phosphorescence of pure organic luminogens. *Chin. Chem. Lett. 27*, 1184-1192.

19. Gong, Y., Tan, Y., Mei, J., Zhang, Y., Yuan, W., Zhang, Y., Sun, J., Tang, B. (2013). Room temperature phosphorescence from natural products: Crystallization matters. *Sci. China Chem. 54*, 1178-1182.

20. Lehner, P., Staudinger, C., Borisov, S. M., and Klimant, I. (2014). Ultra-sensitive optical oxygen sensors for characterization of nearly anoxic systems. *Nat. Commun. 5*, 4460.

21. DeRosa, C. A., Seaman, S. A., Mathew, A. S., Gorick, C, M., Fan, Z., Demas, J. N., Peirce, S. M., and Fraser, C. L. (2016). Oxygen sensing difluoroboron β-diketonate polylactide materials with tunable dynamic ranges for wound imaging. *ACS Sens. 1*, 1366-1373.

22. Chai, Z., Wang, C., Wang, J., Liu, F., Xie, Y., Zhang, Y. -Z., Li, J. -R., Li, Q., and Li, Z. (2017). Abnormal room temperature phosphorescence of purely organic boron-containing compounds: the relationship between the emissive behavior and the molecular packing, and the potential related applications. *Chem. Sci. 8*, 8336-8344.

23. Kuno, S., Akeno, H., Ohtani, H., and Yuasa, H. (2015). Visible room-temperature phosphorescence of pure organic crystals via a radical-ion-pair mechanism. *Phys. Chem. Chem. Phys. 17*, 15989-15995.

24. Smith, M. K., and Northrop. B. H. (2014). Vibrational properties of boroxine anhydride and boronate ester materials: Model systems for the diagnostic characterization of covalent organic frameworks. *Chem. Mater. 26*, 3781-3795.

25. Nagarajan, K., Gopan, G., Cheriya, R. T., and Hariharan, M. (2017). Long alkyl side-chains impede exciton interaction in organic light harvesting crystals. *Chem. Commun. 53*, 7409-7411.

26. Gu, L., Shi, H., Gu, M., Li, K., Ma, H., Cai, S., Song, L., Ma, C., Li, H., Xing, G., et al. (2018). Dynamic ultralong organic phosphorescence by photoactivation. *Angew. Chem. Int. Ed. 57*, 8425-8431.

27. Yang, J., Zhen, X., Wang, B., Gao, X., Ren, Z., Wang, J., Xie, Y., Li, J., Peng, Q., Pu, K., et al.

(2018). The influence of the molecular packing on the room temperature phosphorescence of purely organic luminogens. *Nat. Commun. 9*, 840.

28. Wu, Q., Ma, H., Ling, K., Gan, N., Cheng, Z., Gu, Z., Gu, L., Cai, S., An, Z., Shi, H., et al. (2018). Reversible ultralong organic phosphorescence for visual and selective chloroform detection. *ACS Appl. Mater. Interfaces 10*, 33730-33736.

29. Gao, M., Tian, Y., Yang, J., Li, X., Fang, M., and Li, Z. (2021). The same molecule but a different molecular conformation results in a different room temperature phosphorescence in phenothiazine derivatives. *J. Mater. Chem. C 9*, 15375-15380.

30. Tian, Y., Gong, Y., Liao, Q., Wang, Y., Ren, J., Fang, M., Yang, J., and Li, Z. (2020). Adjusting organic room-temperature phosphorescence with orderly stimulus-responsive molecular motion in crystals. *Cell Rep. Phys. Sci. 1*, 100052.

31. Gu, M., Shi, H., Ling, K., Lv, A., Huang, K., Singh, M., Wang, H., Gu, L., Yao, W., An, Z., et al. (2020). Polymorphism-dependent dynamic ultralong organic phosphorescence. *Research 2020*, 8183450.

32. Deng, Y., Zhao, D., Chen, X., Wang, F., Song, H., and Shen, D. (2013). Long life pure organic phosphorescence based on water soluble carbon dots. *Chem. Commun. 49*, 5751-575.

33. Su, Y., Phua, S. Z. F., Li, Y., Zhou, X., Jana, D., Liu, G., Lim, W. Q., Ong, W. K., Yang, C., and Zhao, Y. (2018). Ultralong room temperature phosphorescence from amorphous organic materials toward confidential information encryption and decryption. *Sci. Adv. 4*, aas9734.

34. Zhang, Y., Gao, L., Zheng, X., Wang, Z., Yang, C., Tang, H., Qu, L., Li, Y., and Zhao, Y. (2021). Ultraviolet irradiation-responsive dynamic ultralong organic phosphorescence in polymeric systems. *Nat. Commun. 12*, 2297.

35. Wang, Y., Li, T., Ma, P., Bai, H., Xie, Y., Chen, M., and Dong, W. (2016). Simultaneous enhancements of UV-shielding properties and photostability of poly(vinyl alcohol) via incorporation of sepia eumelanin. *ACS Sustainable Chem. Eng. 4*, 2252–2258.

36. Louis, M., Thomas, H., Gmeich, M., Haft, A., Fries, F., and Reineke, S. (2019). Blue-light-absorbing thin films showing ultralong room-temperature phosphorescence. *Adv. Mater. 31*, 1807887.

37. Gmelch, M., Thomas, H., Fries, F., and Reineke, S. (2019). Programmable transparent organic luminescent tags. *Sci. Adv. 5*, eaau7310.

38. Wang, C., Zhang, Y., Wang, Z., Zheng, Y., Zheng, X., Gao, L., Zhou, Q., Hao, J., Pi, B., Li, Q., et al. (2022). Photo-induced dynamic room temperature phosphorescence based on triphenyl phosphonium containing polymers. *Adv. Funct. Mater. 32*, 2111941.

39. Yang, Y., Wang, J., Li, D., Yang, J., Fang, M., and Li, Z. (2021). Tunable photoresponsive behaviors based on triphenylamine derivatives: the pivotal role of π-conjugated structure and corresponding application. *Adv. Mater. 33*, 2104002.

40. Wang, Y., Gao, H., Yang, J., Fang, M., Ding, D., Tang, B. Z., and Li, Z. (2021). High performance of simple organic phosphorescence host–guest materials and their application in time-resolved bioimaging. *Adv. Mater. 33*, 2007811.

41. Wang, Y., Yang, J., Fang, M., Gong, Y., Ren, J., Tu, L., Tang, B. Z., and Li, Z. (2021). New phenothiazine derivatives that exhibit photoinduced room-temperature phosphorescence. *Adv. Funct. Mater. 31*, 2101719.

42. Chen, X., Zhong, Q., Cui, C., Ma, L., Liu, S., Zhang, Q., Wu, Y., An, L., Cheng, Y., Ye, S., et al. (2020). Extremely tough, puncture-resistant, transparent, and photoluminescent polyurethane elastomers for crack self-diagnose and healing tracking. *ACS Appl. Mater. Interfaces 12*, 30847-30855.

43. Wang, Z., Zheng, Y., Su, Y., Gao, L., Zhu, Y., Xia, J., Zhang, Y., Wang, C., Zheng, X., Zhao, Y., et al. (2022). Ultraviolet-activated long-lived room-temperature phosphorescence from small organic molecule-doped polymer systems. *Sci. China Mater. 65*, 2160–2168.

44. Mei, J., Leung, N. L. C., Kwok, R. T. K., Lam, J. W. Y., and Tang, B. Z. (2015). Aggregation-induced emission: Together we shine, united we soar! *Chem. Rev. 115*, 11718–11940.

45. Nicol, A., Kwok, R. T. K., Chen, C., Zhao, W., Chen, M., Qu, J., and Tang, B. Z. (2017). Ultrafast delivery of aggregation-induced emission nanoparticles and pure organic phosphorescent nanocrystals by saponin encapsulation. *J. Am. Chem. Soc. 139*, 14792–14799.

46. Zhang, G., Palmer, G., M., Dewhirst, M. W., Fraser, C. L. (2009). A dual-emissive-materials design concept enables tumour hypoxia imaging. *Nat. Mater. 8*, 747-751.

47. Feng, G., and Liu, B. (2018). Aggregation-induced emission (AIE) dots: Emerging theranostic nanolights. *Acc. Chem. Res. 51*, 1404–1414.

48. Jia, X., Shao, C., Bai, X., Zhou, Q., Wu, B., Wang, L., Yue, B., Zhu, H., and Zhu, L. (2019). Photoexcitation-controlled self-recoverable molecular aggregation for flicker phosphorescence. *Proc. Nat. Acad. Sci. U.S.A. 116*, 4816-4821.

49. Xu, J., Feng, H., Teng, H., Chen, G., Pan, S., Chen, J., and Qian, Z. (2018). Reversible switching between phosphorescence and fluorescence in a unimolecular system controlled by external stimuli. *Chem. Eur. J. 24*, 12773-12778.

50. Wu, H., Zhou, Y., Yin, L., Hang, C., Li, X., Agren, H., Yi, T., Zhang, Q., and Zhu, L. (2017). Helical self-assembly-induced singlet–triplet emissive switching in a mechanically sensitive system. *J. Am. Chem. Soc. 139*, 785-791.

51. Villa, M., Roy, M., Bergamini, G., Gingras, M., and Ceroni, P. (2019). A turn-on phosphorescent sensor of Pb^{2+} in water by the formation of a coordination polymer. *Dalton Trans. 48*, 3815-3818.

52. Jia, X., Yue, B., Zhou, L., Niu, X., Wu, W., and Zhu, L. (2020). Fluorescence to multi-colored phosphorescence interconversion of a novel, asterisk-shaped luminogen via multiple external stimuli. *Chem. Commun. 56*, 4336-4339.

53. Weng, T., Zou, Q., Zhang, M., Wu, B., Baryshnikov, G. V., Shen, S., Chen, X., Agren, H., Jia, X., and Zhu, L. (2021). Enhancing the operability of photoexcitation-controlled aggregation-induced emissive molecules in the organic phase. *J. Phys. Chem. Lett. 12*, 6182-6189.

54. Andrew, P., and Barnes, W. L. (2000). Förster energy transfer in an optical microcavity. *Science 290*, 785-788.

55. van der Meer, B. W., van der Meer, D. M., and Vogel, S. S. (2013). Optimizing the orientation factor kappa-squared for more accurate FRET measurements. FRET-Förster Resonance Energy Transfer. Ed.: I. Medintz, N. Hildebrandt, Wiley-VCH Verlag GmbH & Co. KGaA.

56. Sun, Y., Giebink, N. C., Kanno, H., Ma, B., Thompson, M. E., and Forrest, S. R. (2006). Management of singlet and triplet excitons for efficient white organic light-emitting devices. *Nature 440*, 908-912.

57. Busby, E., Xia, J., Wu, Q., Low, J. Z., Song, R., Miller, J. R., Zhu, X. -Y., Campos, L. M., and Sfeir, M. Y. (2015). A design strategy for intramolecular singlet fission mediated by charge-transfer states in donor–acceptor organic materials. *Nat. Mater. 14*, 426-433.

58. Guzelturk, B., and Demir, H. V. (2015) Organic–inorganic composites of semiconductor nanocrystals for efficient excitonics. *J. Phys. Chem. Lett. 6*, 2206-2215.

59. Huang, L., Chen, B., Zhang, X., Trindle, C. O., Liao, F., Wang, Y., Miao, H., Luo, Y., and Zhang, G. (2018). Proton-activated “off–on” room-temperature phosphorescence from purely organic thioethers. *Angew. Chem. Int. Ed. 57*, 16046-16050.

60. Beijonne, D., Yamagata, H., Bredas, J. L., Spano, F. C., and Olivier, Y. (2013). Charge-transfer excitations steer the davydov splitting and mediate singlet exciton fission in pentacene. *Phys. Rev. Lett. 110*, 226402.

61. Ma, X., Wang, J., and Tian, H. (2019). Assembling-induced emission: an efficient approach for amorphous metal-free organic emitting materials with room-temperature phosphorescence. *Acc. Chem. Res. 52*, 738−748.

62. Wu, H., Gu, L., Baryshnikov, G. V., Wang, H., Minaev, B. F., Agren, H., and Zhao, Y. (2020). Molecular phosphorescence in polymer matrix with reversible sensitivity. *ACS Appl. Mater. Interfaces 12*, 20765–20774.

63. Zhang, Y., Wang, Z., Su, Y., Zheng, Y., Tang, W., Yang, C., Tang, H., Qu, L., Li, Y., and Zhao, Y. (2021). Simple vanilla derivatives for long-lived room-temperature polymer phosphorescence as invisible security inks. *Research 2021*, 8096263.

64. Al-Attar, H. A., and Monkman, A. P. (2012). Room-temperature phosphorescence from films of isolated water-soluble conjugated in hydrogen-bonded matrices. *Adv. Funct. Mater. 22*, 3824–3832.

65. Zhang, N., Zhang, B., Pang, Y., Yang, H.-S., Zhong, L., Duan, Y.-X., and Zhang, J.-M. (2022). High performance of PVA nanocomposite reinforced by Janus-like asymmetrically oxidized graphene: Synergetic effect of H-bonding interaction and interfacial crystallization. *Chinese J. Ploym. Sci. 40*, 373-383.

66. Lee, H., Kim, J., Kim, H., Kim, J., and Kwon, S. (2010). Color-barcoded magnetic microparticles for multiplexed bioassays. *Nat. Mater. 9*, 745-749.

67. Lee, J., Bisso, P. W., Srinivas, R. L., Kim, J. J., Swiston, A. J., and Doyle, P. S. (2014). Universal process-inert encoding architecture for polymer microparticles. *Nat. Mater. 13*, 524-529.

68. Zhang, Z., Guo, K., Li, Y., Li, X., Guan, G., Li, H., Luo, Y., Zhao, F., Zhang, Q., Wei, B., et al. (2015). A colour-tunable, weavable fibers-shaped polymer light-emitting electrochemical cell. *Nat. Photon. 9*, 233-238.

69. Huo, M., Dai, X-Y., Liu, Y. (2022). Ultralarge Stokes shift phosphorescence artificial harvesting supramolecular system with near-infrared emission. *Adv. Sci. 9*, 2201523.

70. Huo, M., Dai, X-Y., Liu, Y. (2021). Ultrahigh supramolecular cascaded room-temperature phosphorescence capturing system. *Angew. Chem. Int. Ed. 60*, 27171-27177.

71. Huo, M., Dai, X-Y., Liu, Y. (2022). Uncommon supramolecular phosphorescence-capturing

assembly based on cucurbit[8]uril-mediated molecular folding for near-infrared lysosome imaging. *Small 18*, 2104514.

72. Hu, Y-Y., Dai, X-Y., Dong, X., Huo, M., Liu, Y. (2022). Generation of tunable ultrastrong white-light emission by activation of a solid supramolecule through bromonaphthylpyridinium polymerization. *Angew. Chem. Int. Ed. 61*, e202213097.

73. Mao, Z., Yang, Z., Mu, Y., Zhang, Y., Wang, Y., Chi, Z., Lo, C-C., Liu, S., Lien, A., and Xu, J. (2015). Linearly tunable emission colors obtained from a fluorescent-phosphorescent dual-emission compound by mechanical stimuli. *Angew. Chem. Int. Ed. 54*, 6270-6273.

74. Kim, T. -H., Cho, K. -S., Lee, E. K., Lee, S. J., Chae, J., Kim, J. W., Kim, D. H., Kwon, J. -Y., Amaratunga, G., Lee, S. Y., et al. (2011). Full-colour quantum dot displays fabricated by transfer printing. *Nat. Photon. 5*, 176–182.

75. Gu, L., Shi, H., Bian, L., Gu, M., Ling, K., Wang, X., Ma, H., Cai, S., Ning, W., Fu, L., et al. (2019). Colour-tunable ultra-long organic phosphorescence of a single-component molecular crystal. *Nat. Photon. 13*, 406-411.

76. Su, Y., Zhang, Y., Wang, Z., Gao, W., Jia, P., Zhang, D., Yang, C., Li, Y., and Zhao, Y. (2020). Excitation-dependent long-life luminescent polymeric systems under ambient conditions. *Angew. Chem. Int. Ed. 59*, 9967-9971.

77. Wang, Z., Zhang, Y., Wang, C., Zheng, X., Zheng, Y., Gao, L., Yang, C., Li, Y., Qu, L., and Zhao, Y. (2020). Color-tunable polymeric long-persistent luminescence based on polyphosphazenes. *Adv. Mater. 32*, 1907355.

78. Cai, S., Ma, H., Sho, H., Wang, H., Wang, X., Xiao, L., Ye, W., Huang, K., Cao, X., Gan, N., et al. (2019). Enabling long-lived organic room temperature phosphorescence in polymers by subunit Interlocking. *Nat. Commun. 10*, 4247.

79. Wang, H., Shi, H., Ye, W., Yao, X., Wang, Q., Dong, C., Jia, W., Ma, H., Cai, S., Huang, K., et al. (2019). Amorphous ionic polymers with color-tunable ultralong organic phosphorescence. *Angew. Chem. Int. Ed. 58*, 18776-18782.

80. Gu, L., Wu, H., Ma, H., Ye, W., Jia, W., Wang, H., Chen, H., Zhang, N., Wang, D., Qian, C., et al. (2020). Color-tunable ultralong organic room temperature phosphorescence from a multicomponent copolymer. *Nat. Commun. 11*, 944.

81. Zhang, Y., Zhang, C., Chen, Y., Yu, J., Chen, L., Zhang, H., Xu, X., Liu, Y. (2022).

Photo-controlled reversible multicolor room-temperature phosphorescent solid supramolecular pseudopolyrotaxane. *Adv. Opt. Mater. 10*, 2102169.

82. Wu, H., Chen, Y., Dai, X., Li, P., Stoddart, J. F., Liu, Y. (2019). In situ photoconversion of multicolor luminescence and pure white light emission based on carbon dot-supported supramolecular assembly. *J. Am. Chem. Soc*. *141*, 6583-6591.

83. Lei, Y., Dai, W., Guan, J., Guo, S., Guo, F., Ren, F., Zhou, Y., Shi, J., Tong, B., Cai, Z., et al. (2020). Wide-range color-tunable organic phosphorescence materials for printable and writable security inks. *Angew. Chem. Int. Ed. 59*, 16054-16060.

84. Chen, J., Yu, T., Ubba, E., Xie, Z., Yang, Z., Zhang, Y., Liu, S., Xu, J., Aldred, M. P., and Chi, Z. (2019). Achieving dual-emissive and time-dependent evolutive organic afterglow by bridging molecules with weak intermolecular hydrogen bonding. *Adv. Opt. Mater. 7*, 1801593.

85. Wang, J. -X., Fang, Y. -G., Li, C. -X., Niu, L. -Y., Fang, W. -H., Chi, G., and Yang, Q.-Z. (2020). Time-dependent afterglow color in a single-component organic molecular crystal. *Angew. Chem. Int. Ed. 59*, 10032-10036.

86. Dou, X., Zhu, T., Wang, Z., Sun, W., Lai, Y., Sui, K., Tan, Y., Zhang, Y., and Yuan, W. Z. (2020). Color-tunable, excitation-dependent, and time-dependent afterglows from pure organic amorphous polymers. *Adv. Mater. 32*, 2004768.

87. Miao, Y., Liu, S., Ma, L., Yang, W., Li, J., and Lv, J. (2021). Ultralong and color-tunable room-temperature phosphorescence based on commercial melamine for anticounterfeiting and information recognition. *Anal. Chem. 93*, 4075–4083.

88. Mao, Z., Yang, Z., Fan, Z., Ubba, E., Li, W., Li, Y., Zhao, J., Yang, Z., Aldred, M. P., and Chi, Z. (2019). The methylation effect in prolonging the pure organic room temperature phosphorescence lifetime. *Chem. Sci. 10*, 179-184.

89. Tao, Y., Chen, R., Li, H., Yuan, J., Wan, Y., Jiang, H., Chen, C., Si, Y., Zheng, C., Yang, B., et al. (2018). Resonance-activated spin-flipping for efficient organic ultralong room-temperature phosphorescence. *Adv. Mater. 30*, 1803856.

90. Li, H., Li, H., Gu, J., He, F., Peng, H., Tao, Y., Tian, D., Yang, Q., Li, P., Zheng, C., et al. (2021). Fluorine-induced aggregate-interlocking for color-tunable organic afterglow with a simultaneously improved efficiency and lifetime. *Chem. Sci. 12*, 3580-3586.

91. She, P., Lu, J., Qin, Y., Li, F., Wei, J., Ma, Y., Wang, W., Liu, S., Huang, W., and Zhao, Q. (2021).

Controllable photoactivated organic persistent room-temperature phosphorescence for information encryption and visual temperature detection. *Cell Rep. Phys. Sci. 2*, 100505.

92. He, Z., Zhao, W., Lam, J. W. Y., Peng, Q., Ma, H., Liang, G., Shuai, Z., and Tang, B. Z. (2017). White light emission from a single organic molecule with dual phosphorescence at room temperature. *Nat. Comm. 8*, 416.

93. Tani, Y., Terasaki, M., Komura, M., and Ogawa, T. (2019). Room-temperature phosphorescence-to-phosphorescence mechanochromism of a metal-free organic 1,2-diketone. *J. Mater. Chem. C 7*, 11926-11931.

94. Mukherjee, S., and Thilagar, P. (2015). Recent advances in purely organic phosphorescent materials. *Chem. Commun. 51*, 10988-11003.

95. Ito, S., Taguchi, T., Yamada, T., Ubukata, T., Yamaguchi, Y., and Asami, M. (2017). Indolylbenzothiadiazoles with varying substituents on the indole ring: a systematic study on the self-recovering mechanochromic luminescence. *RSC Adv. 7*, 16953-16962.

96. Wu, H., Wang, D., Zhao, Z., Wang, D., Xiong, Y., and Tang, B. Z. (2021). Tailoring noncovalent interactions to activate persistent room-temperature phosphorescence from doped polyacrylonitrile films. *Adv. Funct. Mater. 31*, 2101656.

97. Garain, S., Garain, B. C., Eswaramoorthy, M., Pati, S. K., and George, S. J. (2021). Light-harvesting supramolecular phosphors: highly efficient room temperature phosphorescence in solution and hydrogels. *Angew. Chem. Int. Ed. 60*, 19720-19724.

98. Gao, L., Zhang, Y., Chen, X., Zheng, Y., Zheng, X., Wang, C., Wang, Z., Hao, J., Tian, Q., Yu, X., et al. (2021). Water-induced blue-green variable nonconventional ultralong room temperature phosphorescence from cross-linked copolymers via click chemistry. *Adv. Opt. Mater. 9*, 2101284.

99. Kwon, M. S., Lee, D., Seo, S., Jung, J., and Kim, J. (2014). Tailoring intermolecular interactions for efficient room-temperature phosphorescence from purely organic materials in amorphous polymer matrices. *Angew. Chem. Int. Ed. 53*, 11177-11181.

100. Cai, S., Sun, Z., Wang, H., Yao, X., Ma, H., Jia, W., Wang, S., Li, Z., Shi, H., An, Z., et al. (2021). Ultralong organic phosphorescent foams with high mechanical strength. *J. Am. Chem. Soc.* 143, 16256-16236.